School of Medicine

University of Crete

Master program in Neurosciences

IMBB-FoRTH, eflab, Emmanouil Froudarakis

Diploma thesis

Functional connectivity and topographic organization across mouse visual areas

Athanasios Vavoulis

Supervisor: Emmanouil Froudarakis

Heraklion

2022

Examination Committee

Emmanouil Froudarakis

IMBB Group Leader, Assistant Professor Grade

Maria Papadopouli

Professor of Computer Science, University of Crete

Panayiota Poirazi

Director of Research at IMBB-FORTH

Curriculum Vitae (CV)

Education

- Postgraduate student in Neurosciences, University of Crete, 2019 - until now

Calculated degree until now (9,44)

- Medical degree, University of Crete, 2013-2019

Degree (7,66)

Experience

- Statistical analysis of two-photon imaging data of mice in lab of Emmanouil Froudarakis in IMBB-FoRTH on functional parcellation of visual cortex, 2020 – 2022.
- Statistical analysis of clinical data of patients with schizophrenia and bipolar disease in psychiatric clinic Agios Charalampos on predicting treatment resistance and relapses in a 2-year follow-up, 2020 – in progress.
- BCI classification models on EEG data, LaSEEB, Lisbon, 2022 – in progress.

Foreign Languages

- **English :** Certificate of Proficiency (ECPE), Michigan
- **French :** Diplome des estudes en la langue francaise (delf B2)

Abstract

A fundamental process towards understanding the visual system is the precise characterization of the topographic arrangement of visual cortical areas. Although the interpretation of cortical circuits in primates is considerably more comprehensible due to the resemblance with human brain, mice present many advantages for the study of neural functions as an experimental animal model. Its effortless breeding (i.e. short generation time, pregnancy length and lifespan) and easy genetic manipulations, enables the application of sophisticated imaging techniques, the modelling of human diseases and the intervention in molecular pathways (Laramée and Boire 2015). Therefore, mice offer significant benefits over larger mammals in order to gain insight into the operations mediated by brain networks.

The detailed parcellation of mouse visual cortex rely on architectonic changes. However, describing the anatomical differences between visual areas is a difficult procedure. Therefore, many studies attempted to discover functional properties that would segregate the regions of visual cortex. On the premise that each visual area represents a retinotopic copy of visual space and due to the mirroring representations of visual field in neighboring areas, the boundaries could also be defined by the reversal of retinotopic gradients (Marshel et al. 2011), (Garrett et al. 2014). However, this methodology raises substantial challenges which emerge from the wide distribution of retinotopic information in the transitions of visual areas. As a consequence, the manual delineation of retinotopic borders is not trivial. In addition, an important issue for the validity of retinotopic maps is the mismatch between retinotopic and anatomical borders (Zhuang et al. 2017).

In this study, an attempt was made to improve the characterization of boundaries between neighboring areas of mouse visual cortex by studying the functional connectivity of neurons. Under the assumption that interactions of cells within the same region are expected to be stronger than with cells of different regions, two-photon imaging recordings of the visual cortex during the passive presentation of movies were used to classify neurons into different visual areas based on their functional connectivity. The resulting functional map revealed (i) shifted borders relative to the retinotopic, with higher order-areas expanded towards the V1 patch and (ii) regions of heterogeneous membership along the borders. The analysis of correlations across the border displayed that (i) the topography of functional connections coincides with the centers of the associated visual areas and (ii) the magnitude of neural

interactions diminishes close to the boundary. These results were suggestive of the functional segmentation of visual areas.

Since the anatomical borders were not available, additional functional parameters were employed for evaluating and contrasting the connectivity and retinotopic arrangement of visual cortex. These functional properties were (i) reliability, (ii) state dependence and (iii) response decay timescale.

As a conclusion, the analysis showed that functional connectivity could be a valuable tool for describing the area membership. However, since retinotopic, anatomical and functional connectivity exhibit important differences at the delineation of borders, further investigations need to be made in order to have a more precise characterization of the area membership of border cells.

Keywords

Connectivity, correlations, noise, signal, retinotopy, map, visual area, border cell, center cell, organization, dimensionality reduction, directionality, reliability, state dependence, response decay timescale.

Περίληψη

Μια θεμελιώδης διαδικασία για την κατανόηση του οπτικού συστήματος είναι ο ακριβής χαρακτηρισμός της τοπογραφικής διάταξης των περιοχών του οπτικού φλοιού. Η χαρτογραφηση του οπτικού φλοιού του ποντικιού βασίζεται σε αρχιτεκτονικές αλλαγές. Ωστόσο, η περιγραφή των ανατομικών συνόρων των οπτικών περιοχών είναι μια δύσκολη διαδικασία. Ως εκ τούτου, πολλές μελέτες προσπάθησουν να ανακαλύψουν λειτουργικές ιδιότητες που θα διαχωρίζουν τις περιοχές του οπτικού φλοιού. Με την προϋπόθεση ότι κάθε οπτική περιοχή αντιπροσωπεύει ένα αντίγραφο του οπτικού χώρου και λόγω των κατοπτρικών αναπαραστάσεων του οπτικού πεδίου σε γειτονικές περιοχές, τα όρια θα μπορούσαν να οριστούν από την αναστροφή της αμφιβληστροειδοτοπικών κλίσης. Ωστόσο, αυτή η μεθοδολογία εγείρει σημαντικές προκλήσεις που προκύπτουν από την ευρεία διανομή της αμφιβληστροειδοτοπικής πληροφορίας στη μετάβαση των οπτικών περιοχών. Κατά συνέπεια, η χειροκίνητη οριοθέτηση των αμφιβληστροειδοτοπικών ορίων δεν είναι ευκολη διαδικασια. Επιπλέον, ένα σημαντικό ζήτημα για την εγκυρότητα των αμφιβληστροειδοτοπικών χαρτών είναι η αναντιστοιχία τους με τα όρια που προτείνονται από ανατομικά δεδομένα.

Σε αυτή τη μελέτη, έγινε μια προσπάθεια να βελτιωθεί ο χαρακτηρισμός των ορίων μεταξύ γειτονικών περιοχών του οπτικού φλοιού μελετώντας τη λειτουργική συνδεσιμότητα των νευρώνων. Σύμφωνα με το γεγονός ότι οι αλληλεπιδράσεις των κυττάρων στην ίδια περιοχή είναι ισχυρότερες σε σχέση με κύτταρα διαφορετικών περιοχών, χρησιμοποιήθηκαν καταγραφές του οπτικού φλοιού κατά την παθητική παρακολούθηση ταινιών, για την ταξινόμηση των νευρώνων με βάση τη λειτουργική τους συνδεσιμότητα. Ο λειτουργικός χάρτης που προέκυψε αποκάλυψε μετατοπισμένα σύνορα σε σχέση με τα αμφιβληστροειδοτοπικά και περιοχές ετερογενούς ταυτοτητας κατά μήκος των συνόρων. Συμπερασματικά, η λειτουργική συνδεσιμότητα των νευρώνων θα μπορούσε να είναι ένα πολύτιμο εργαλείο για την περιγραφή των συνόρων των περιοχών.

Contents

Abbreviations

Visual areas; AL: anterolateral area, AM: anteromedial area, LI: laterointermediate area, LM: lateromedial area, V1: primary visual cortex, P: posterior area, PM: posteromedial area, RL: rostrolateral area.

LDA: Linear Discriminant Analysis

PCA: Principal Component Analysis

NB: Naïve Bayes

SVM: Support Vector Machine

t-SNE: t-distributed stochastic neighbor embedding

ROC: Receiver Operating Characteristic

AUC: Area Under the Curve.

Chapter 1. Introduction

Visual cortex consists of interconnected areas which correspond to topographically organized assemblies of neurons with comparable anatomical and functional properties. The precise description of areal boundaries is a vital process towards the complete assessment of visual cortex parcellation. Innovative investigations have segmented mouse posterior cortex using architectonic features (Olavarria and Montero 1989), tract tracing methods (Q and A 2007) and retinotopy (Schuett, Bonhoeffer, and Hübener 2002), (Kalatsky and Stryker 2003), (JH et al. 2011). Architectonic maps are constructed based on changes in cell density, whereas functional maps attempt to uncover the distinct mechanisms behind the flow of visual information.

The prevailing functional attribute for defining the spatial arrangement of visual cortical areas is retinotopy, which provides a method for distinguishing visual areas based on their visuotopic organization. The orderly sequence of the visual stream from retina to visual cortex, which emerges from connections between neurons in different parts of the visual system, preserves the spatial organization of cell structures into visual field maps. Therefore, each visual area contains a complete map of the visual field. In fact, due to the mirroring representations of visual field in neighboring areas, retinotopic borders can be determined by the reversals in the retinotopic gradients (Marshel et al. 2011). In addition, a previous study developed an automated image analysis approach which identifies patches of positive and negative values indicative of a non-mirror and mirror representation, respectively (Garrett et al. 2014).

However, interpreting the organization of visual cortex from retinotopy is especially challenging. At first, the transitions of visual areas are characterized by wide distributions of retinotopic information. For instance, neurons' azimuth reversal in V1-LM margin requires several hundreads μm to complete (Zhuang et al. 2017). Given that areal boundaries are delineated manually at the location of retinotopic reversal, it is almost impossible to draw an objective border between visual areas. Moreover, mouse higher-order visual areas lack a full representation of the visual field and over-represent particular regions of visual space (Garrett et al. 2014). The representational bias of a given visual area is typically correlated with the region mapped onto the neighboring portion of V1, leading to overlapping visual field coverage profiles of neighboring visual areas (Garrett et al. 2014). As a result, regions nearby the borders are defined by a mixture of functional properties, leading to overlapping visual areas. Another

important issue for retinotopy is the mismatch revealed among retinotopic and anatomical borders (Zhuang et al. 2017).

Therefore, much work has been devoted to identify the distinct properties of higher order areas. In this direction, many studies have examined the neural responses to variable visual stimuli. From simple presentations of drifting gratings with variable spatial and temporal frequency or orientation, to complex movies with wealthy spatiotemporal statistics, multiple functional properties have proven the discrepancies that exist across different cortical areas (Siegle et al. 2021), (Glickfeld et al. 2013), (Fahey et al. 2019), (Piasini et al. 2021), (Andermann et al. 2011).

On the other hand, many researchers simply support that adjacent neurons are more functionally similar than distant ones and that visual cortex of mice is organized as a continuum of functional arrangement where encoding similarities reduces gradually over space (Song, Kennedy, and Wang 2014). As a result, a smooth functional organization could explain both the apparent discrepancies and similarities of cells with spatial proximity. This is consistent with previous work which suggests that parietal and retrosplenial areas lack internal anatomical boundaries (Gămănuţ et al. 2018).

Since sensory encoding of various stimuli displayed such complications for segmenting visual areas, the interest oriented to neuronal structures established by functional connectivity. It has been proven that connection probability is elevated for neurons responding similarly to identical stimuli (Ko et al. 2011). Therefore, since neurons that share common attributes reside close to each other, functional connectivity would be greater for adjacent cells and decay with anatomical distance (Harris and Mrsic-Flogel 2013), (Song et al. 2014).

However, the cortical regions close to the boundaries of visual areas are much less characterized. It is unknown whether cells near the border and at the center of visual areas display the same connectivity patterns. Nonetheless, it is true that two neurons are more likely to be connected when they both receive input from common neighbors (Perin, Berger, and Markram 2011). Hence, cells of distinct visual areas close to borders are expected to exhibit lower connection probability, since the afferent projections are distinct for each area (Juavinett et al. 2020).

The goal of this study is to identify the spatial layout and boundaries of mouse visual cortical areas based on the functional connectivity of neurons. Functional connectivity is usually estimated as the Pearson's correlation coefficient between the activity of neuronal pairs

(Cohen and Kohn 2011). In addition, several studies have provided evidence for the importance of correlations in decoding neuronal responses (Averbeck, Latham, and Pouget 2006), (Nirenberg and Latham 2003). Therefore, distinct patterns of functional connectivity could correspond to unique visual structures.

Correlations between neural activities can arise due to multiple sources. In literature, the term 'signal' is used to define if the source is the stimulus, and 'noise' if it is not. Therefore, while 'signal' correlations measure the co-modulation of neural activity in reference to the features of the stimulus, 'noise' estimates the common inconsistencies of the responses to identical stimuli. Neurons do not just encode visual stimulus, but integrate the sensory input with contextual information. As a result, trial-to-trial variability in the activity of neurons is the effect of intrinsic factors and cognitive states, such as reward, learning, attention and arousal (Cohen and Maunsell 2009), (Vinck et al. 2015), (Gu et al. 2011), (Ecker et al. 2010). On the other hand, similarity in stimulus-derived responses of the cells is computed as the correlation of the mean activity of neurons across trials. Nevertheless, the interpretation of neural computations are much more complicated, since the definite discrimination of these two operations is not feasible.

In order to generate an algorithm that could predict the label of neurons next to the border, principal component analysis (PCA) and linear discriminant analysis (LDA) were applied as dimensionality reduction techniques to determine a temporal subspace which discriminates neurons based on their correlation (see Methods). This process was effective due to the ability of PCA to identify the orthogonal projection of the data into a lower dimensional linear space with maximum variance. Taking into account that intra-area correlation are higher than inter-area, a classification method would identify a separation among neurons with diverging responses (Kumar et al. 2021). The predictions of the decoder constructed a functional connectivity map with important differences at the areal boundaries, compared to retinotopic borders. The most exciting finding was the consistency of the border location in varying depths of brain cortex. It is important to report that only 'noise' correlations could arrange the regions of visual cortex. On the other hand, 'signal' correlations might be affected by the common properties of border cells with the training samples of higher order areas. Concretely, an important influence could be the retinotopic information, potentially due to the distinct cortical magnification describing each visual area. Finally, various functional properties were

evaluated in order to examine the possibility of being lined up to the map generated by connectivity.

Chapter 2. Results

Chapter 2.1 Functional Connectivity map and properties of correlations

Chapter 2.1.1 Retinotopic map

Functional connectivity patterns in visual cortex are characterized by within- and cross-area interactions. Here, the goal is to assess the role of population dynamics in the discrimination of retinotopic areas. First of all, the retinotopic maps were constructed according to Garrett et al. 2014 and JH et al. 2011 algorithms. Borders were determined based on horizontal and vertical retinotopy reversals (Figure 1A, 1B). However, due to the wide distribution of retinotopic information in the border regions, the manual delineations of boundaries based on azimuth is not unique (Figure 1C, 1D).

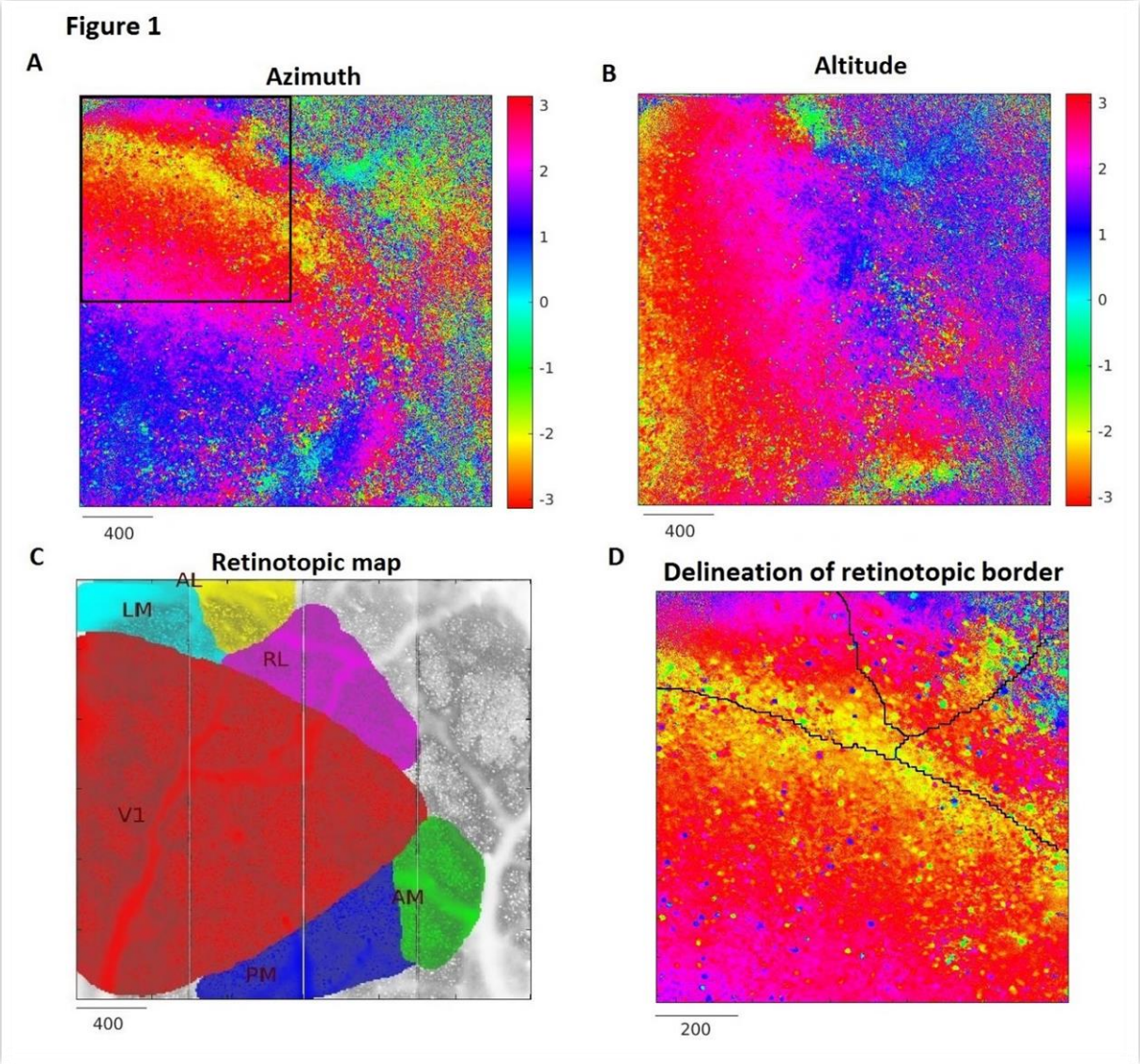

Figure 1. Segmentation of visual cortex by defining visual area patches from retinotopic maps.

A, Example map of horizontal retinotopy (azimuth), in radians of visual space. Nasal field represented by negative values, while temporal periphery by positive. The outlined region indicate the region of D. B, Map of vertical retinotopy (altitude). Upper field represented by negative and lower by positive values. C, Retinotopic map generated by the reversals of retinotopy. D, Expand view of the region with horizontal retinotopy transitions between areas V1, LM, RL and AL. The azimuth reversals are not clear. The black lines determine the drawn retinotopic borders. The dimensions of the scans are determined by 2400 x 2400 μm. The angle is calculated as the angle of the Fourier transform spectrum and normalized for the edges of the screen where the drifting bars are presented.

Chapter 2.1.2 Functional Connectivity map

Next, simultaneous recordings of thousands neurons in V1 and higher-order-areas (AL, LM, RL, PM, AM) with wide-field GCaMP6 imaging were performed in awake, head-fixed mice during the visual stimulation with repeated movies. Data obtained by the movie presentation tasks were utilized for the generation of functional connectivity maps.

A serious impediment to neuroscience is the confrontation of the multiple dimensions of neural data (i.e. *neurons* x *time* x *trials* for each session). Two commonly used approaches to investigate interactions among neurons, while simultaneously reducing the dimensionality of the data, are (i) 'trial-averaged PCA' (Figure 2A) and (ii) 'trial-concatenated PCA' (Figure 2B), (Williams et al. 2018), (Kumar et al. 2021). The first procedure contributes to assess the

stimulus-driven responses, by averaging across identical-stimulus trials, whereas the second operation is utilized for the computation of trial-to-trial variability ('noise').

PCA decompose the initial data by computing the eigenvectors of the covariance matrix. Next, it projects the data to the linear transformation of K dimensions (where $K < D$, D is the number of total temporal dimensions), (Figure 2). In this model, the number of the retained components was chosen in reference to 95% of the explained variance ratio. Indicatively, the 'trial-averaged PCA' reduced the dimensionality from 300 to ~80, whereas the 'trial-concatenated PCA' from 6000 to ~2200. As a result, PCA captures the temporal components with the maximum covariance across neurons. This approach identifies the activity patterns of correlated neurons and project the data to a space which effectively distinguishes uncorrelated population responses. Considering that intra-area correlations outperform inter-area, it is expected that neurons with similar responses would be assigned to the same visual area (Ganesh Kumar et al. 2021).

Next, LDA was incorporated into the algorithm and applied to the output of PCA, with the intention of amplifying the discrimination between the visual areas. In contrast to PCA, LDA is a supervised dimension reduction technique which uses the class labels to find a linear projection that discriminates neurons based on their retinotopic mask. The resulted matrix was described by *N*-neurons x *L*-features, where *L* equals with the number of visual areas minus one. Training samples were chosen in such a manner that only a set of cells was employed for the identification of LDA subspace and the retinotopic information would be restricted to the minimum level. For this purpose, the training set was composed by neurons located away from the border and predictions of Naive Bayes (NB) classifier were made for cells close to the retinotopic borders (see Methods). These operations enabled the estimation of the border organization based on neural correlations.

NB predictions were significantly influenced by the procedures applied before PCA, as 'signal' and 'noise' of neurons in 'trial-averaged PCA' and 'trial-concatenated PCA', respectively, resulted in differing outcomes. The predictions that were made based on dissimilarities in 'signal' correlations among border cells of neighboring areas were fuzzy diverging significantly from the retinotopic map (Figure 2A), while 'noise' correlation-derived predictions generated a functional map corresponding to borders closer to the ones from the retinotopic map and consequently more likely to reflect true anatomical borders (Figure 2B).

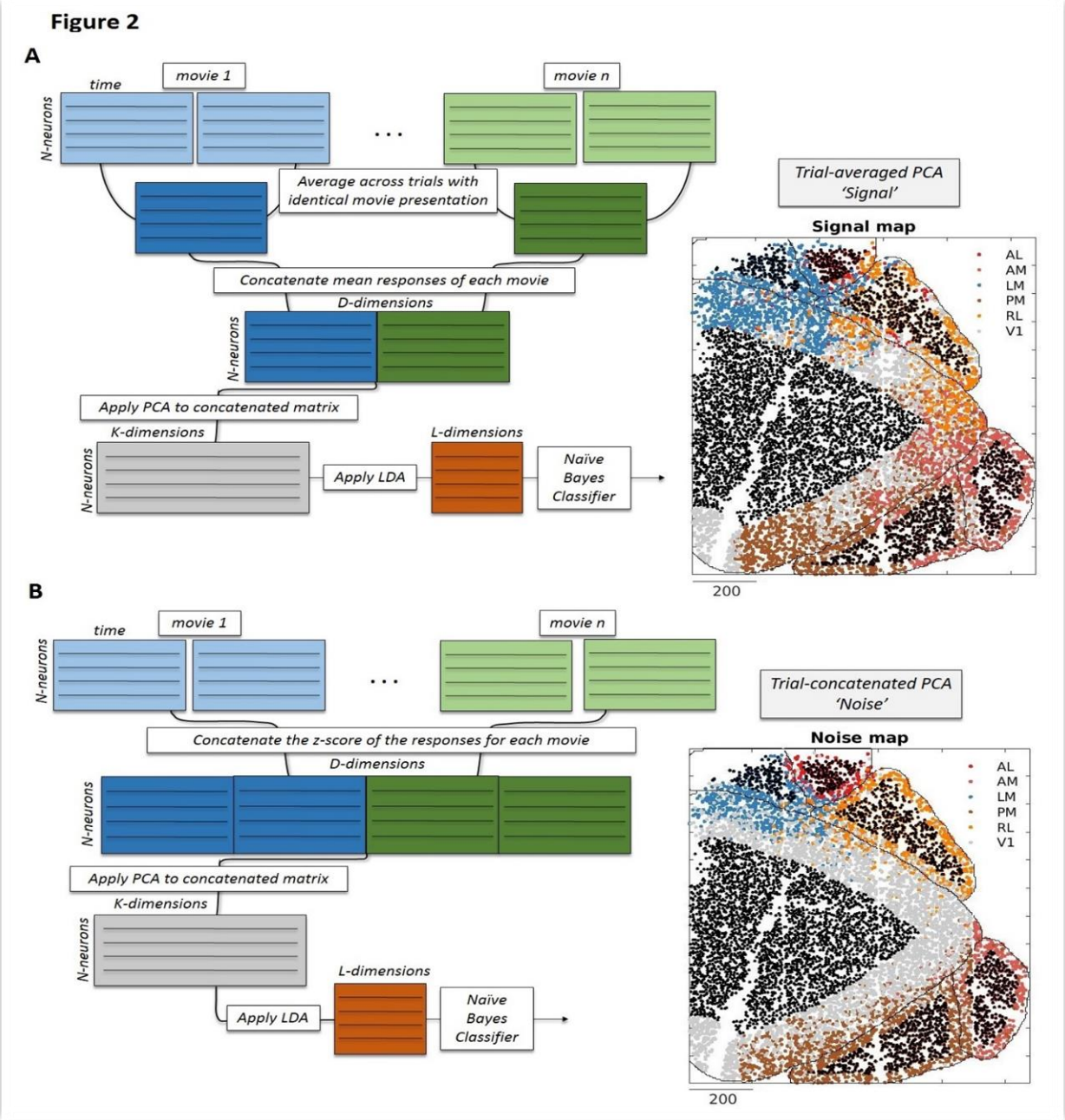

Figure 2. PCA algorithms for the generation of 'signal' and 'noise' correlation-driven maps.

A, 'Trial-averaged PCA' model. Step 1: Averaging across trials with identical stimulus. Step 2: Concatenate all trials. Step 3: PCA for the extraction of components that explain 95% of total variance. Step 4: LDA to the lower-dimension space. Step 5: NB predictions for the border cells. B, 'Trial-concatenated PCA' model. Same steps as above but with a difference in the preprocessing of Step 1: z-score normalization of the firing rate of trials with identical stimulus. Black cells define the training set. Colors determine the prediction of NB (grey: V1, blue: LM, orange: RL, brown: PM, red: AL, "roofing-tile" color: AM). Black lines represent the retinotopic borders. Black bars describe the size of the scan in pixels (pixel = 2 x 2 μm).

In order to gain more insight into the mathematical procedures, the average correlation between cells within and across visual areas were estimated. In every condition, mean correlations within visual areas exceeded the correlations calculated across the visual areas with the ratio of the intra- to inter-area correlations both for 'signal' and 'noise' data being larger than 1 (Figure 3). In contrast to 'noise' ratio, which was amplified due to the preprocessing of PCA+LDA algorithm, 'signal' ratio was diminished for the computations performed at the LDA features (Figure 3B, 3D).

With the intention of evaluating the ability of PCA+LDA to represent the regional correlations, an attempt was made to assess the divergence between intra and inter-area correlations. For this purpose, the F-statistic was the accurate measure. The F-statistics denoted an increase of dispersion between intra- and inter-area 'noise' correlations after the application of the PCA+LDA algorithm. In contrast, the opposite effect was induced by 'signal' correlations (Figure 3D). As a result, 'signal' correlation within visual areas were not sufficiently discriminated from correlations across visual areas, in order to generate a space where neurons of different visual areas could be distinguished.

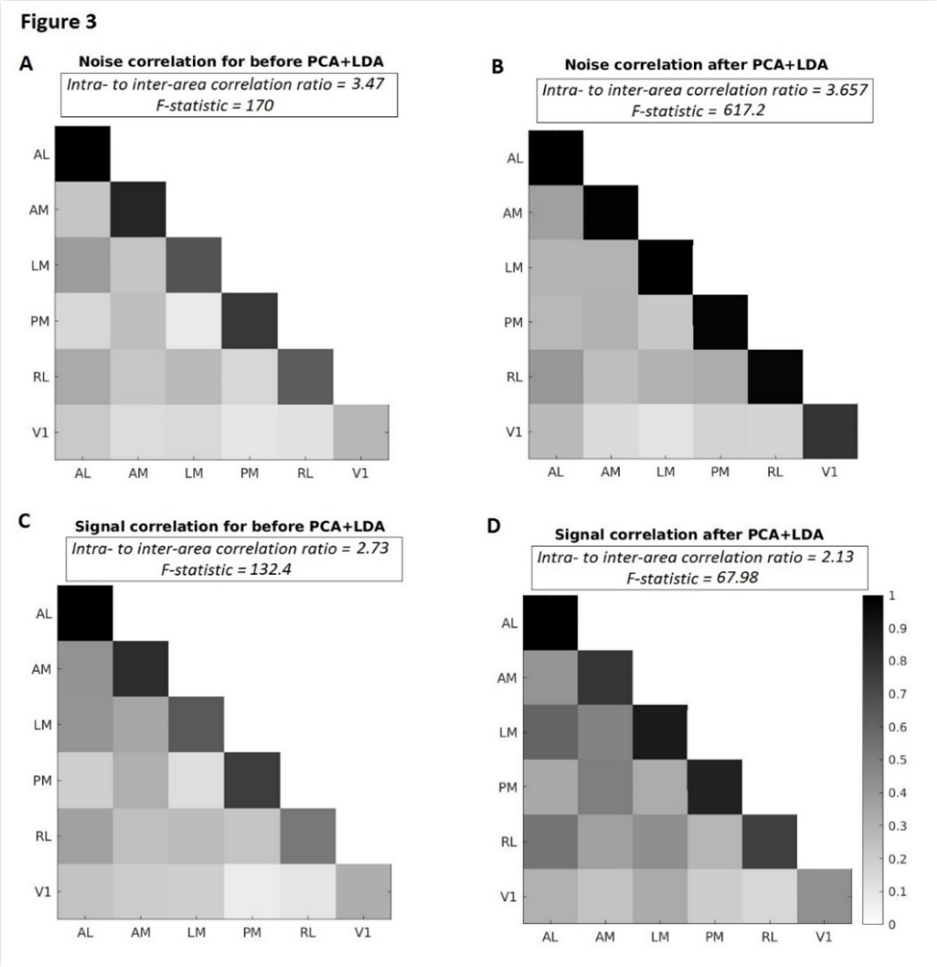

Figure 3. Intra- and inter-area correlations computed on 'signal' and 'noise' data.

Intra-area correlations are satisfactory for the establishment of connectivity maps only in 'noise' data. A, 'Noise' correlations before the application of PCA and LDA. B, Correlations for the LDA features. Augmentation of both 'noise' ratio and F-statistics of ANOVA after the application of PCA+LDA algorithm. C, D, 'Signal' correlations before (left) and after (right) PCA+LDA. Both measures of comparison for the intra- and inter-area correlations (i.e. 'signal' ratio and F-statistics) were diminished after the application of PCA+LDA algorithm. 'Noise' metrics in the "raw" data (A) were superior to the 'signal' calculations (C). Correlations are calculated for the training set located distant from the retinotopic borders. Correlations are normalized between 0 and 1, in order to compare accurately variable data. It is important to mention that in many situations of inter-area correlations the values were negative before the normalization. In all cases, a statistical significance among intra- and inter-area correlations was identified for all scans (ANOVA: p-value < 0.01).

A reasonable assumption is that 'signal' of adjacent cells on the edges of visual areas cannot be clearly separated due to common azimuth, as V1 and LM border cells are defined by similar horizontal retinotopy (Figure 1C). On the other hand, factors that influence the co-fluctuations of neurons ('noise') such as top-down regulation, affect each visual area in a distinct manner, sufficient to establish a map resembling the retinotopic. Based on the correlation[1]-driven topographic arrangement of visual areas, the boundaries exhibited mixed neural membership and shifted boundaries relative to the retinotopic border (Figure 2B). However, further computations are required to assess the underpinnings of these findings.

Chapter 2.1.3 Functioinal connectivity map represents neural correlations better from retinotopic map

To evaluate the organization emerged from functional connectivity and retinotopy, a comparison was made between the mean correlations of border cells with neurons of the

[1] Correlation is referring to 'noise' correlation from now on, unless it is defined by 'signal'.

same class in reference to the retinotopic and correlation-driven arrangement of visual cortex. The results provide evidence that border cells manifest higher correlations for the connectivity-defined visual areas (Figure 4A). This effect of functional connectivity was more robust for the correlations computed in LDA features, as the divergence from the null hypothesis of equivalent correlations for the retinotopic and correlation-driven areas increased after the PCA+LDA algorithm (Figure 4B). Specifically, the distribution of correlations differences among connectivity and retinotopy labels skewed in the direction of the correlation-driven areas (Figure 4B). Apart from this, it is demonstrated that neural correlations were organized in manner which distinguished the neurons of differing visual areas. It seems like V1 neurons were indicated by correlations of inferior magnitude in comparison to higher-order areas (Figure 4B).

So far, it is shown that border cells exhibited stronger interactions with the neurons of identical connectivity-based labels rather than the retinotopic assignment. These findings are in support for the validity of the PCA+LDA algorithm to construct structures of prominent connectivity. However, the quantification of neural interactions with the aim of not only contrasting cells assigned to opposing visual areas, but also identifying the separation rule of the NB classifier has not been established.

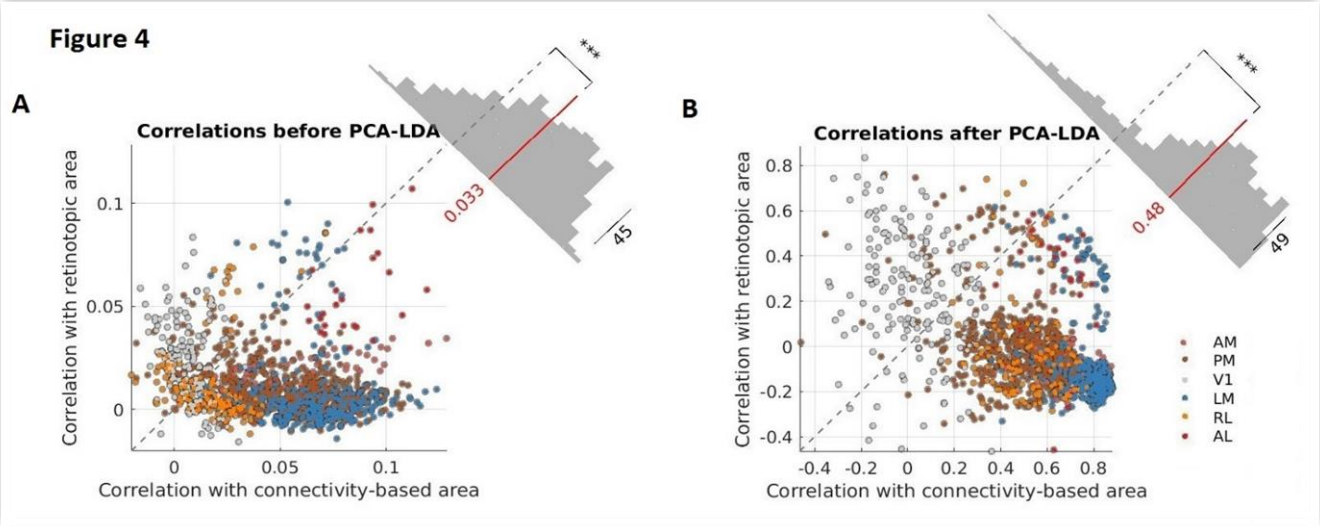

Figure 4. Properties of border cells.

'Noise' correlations of border cells were greater for the correlation-driven organization compared to retinotopic. A, B, Correlations computed before (A) and after (B) applying the 'trial-concatenated PCA' model. In both cases, connectivity of border cells is stronger with the connectivity-defined area (t-test: p-value < 0.01). This phenomenon is amplified for the correlations computed in LDA features (B). The color of each dot represents the class of each cell in reference to connectivity-driven maps.

In this framework, further investigations were conducted with the intention of comparing cells close to the center of each area (training neurons) and adjacent to the border (testing neurons). Center cells had significantly higher correlations compared to border cells and this effect was evident across all areas (Figure 5A-5C). Moreover, the amplitude of correlations varied among visual areas, revealing a distinct influence of 'noise' across different visual areas (Figure 5A-5C). A potential hypothesis could be that this divergence is the motivating power of the decoder for discriminating border cells.

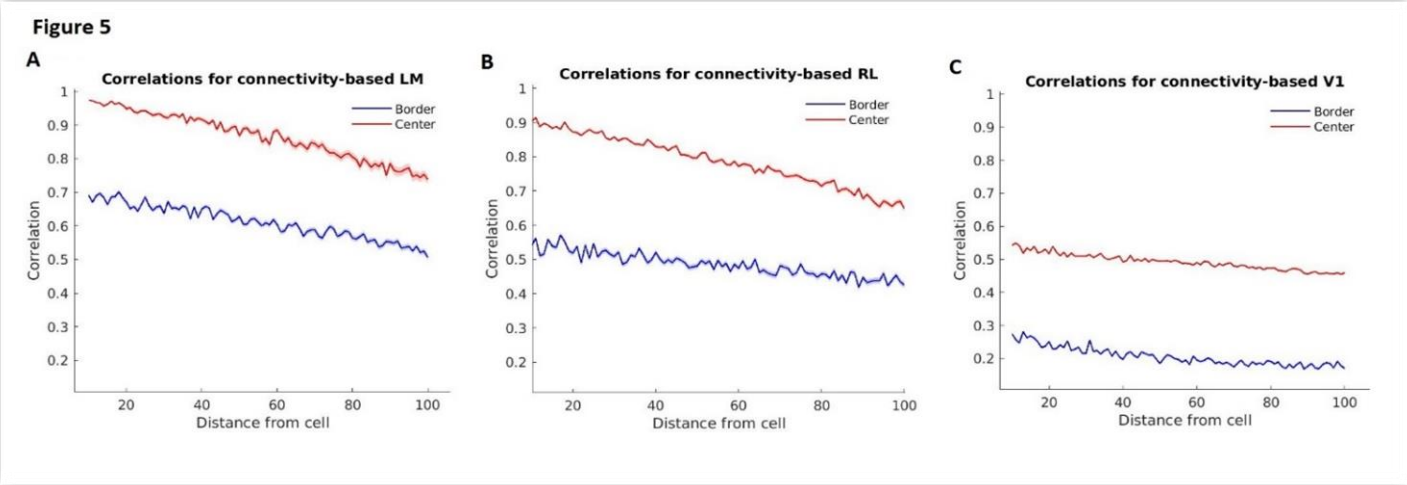

Figure 5. Unique influence of state on 'noise' correlations of each area.

A (LM), B (RL), C (V1), Correlation of border (red) and center (blue) cells for each visual area as a function of distance. Center cells consistently exhibit greater correlations from border cells. Shaded areas around the solid line of mean correlations represents the standard error. Distance is measured in pixels (pixel = 2 x 2 μm).

However, the underlying cause for the higher level of correlations identified within the core of each area compared to regions nearby the margins is not clear. In contrast to center neurons, border cells are adjacent to units of different visual areas. As a result, the correlations computed in Figure 5 for the border cells include the weak interactions of neurons in different visual areas. It is demonstrated that correlations of border cells with the same NB predicted label were stronger than those with opposing classes for LM and RL (Figure 6B, 6C, blue and red line).

In order to compare the retinotopic and connectivity-based organization of borders, correlations were computed as before, but this time by accounting the retinotopic labels. Correlations between cells within the same retinotopic patch were designated by inferior correlations compared to correlations computed in reference to the connectivity-based organization (Figure 6B, 6C, light blue and blue line). In addition, correlations between cells within different retinotopic regions were greater from the corresponding correlations which accounted the connectivity organization (Figure 6B, 6C, yellow and red line). As a result, connectivity map represents neural correlations better from retinotopic map.

Curiously, an attempt for generalizing this pattern across all visual areas had controversial outcome for the retinotopic organization of border cells. Neurons of opposing classes exhibited higher interactions (Figure 6A, yellow line). Similar results were observed for V1 neurons. In addition to the inconclusive correlations for the retinotopic organization, V1 cells also exhibited greater connectivity for the opposing correlation-driven areas compared to the similarly defined areas (Figure 6D, red and blue line, respectively). However, considering the immoderate imbalance among V1 and higher-order areas correlations, it is evident that computations for V1, and by extension all areas, were contaminated by the stronger interactions between neurons from higher-order areas (Figure 5A-5C).

Figure 6

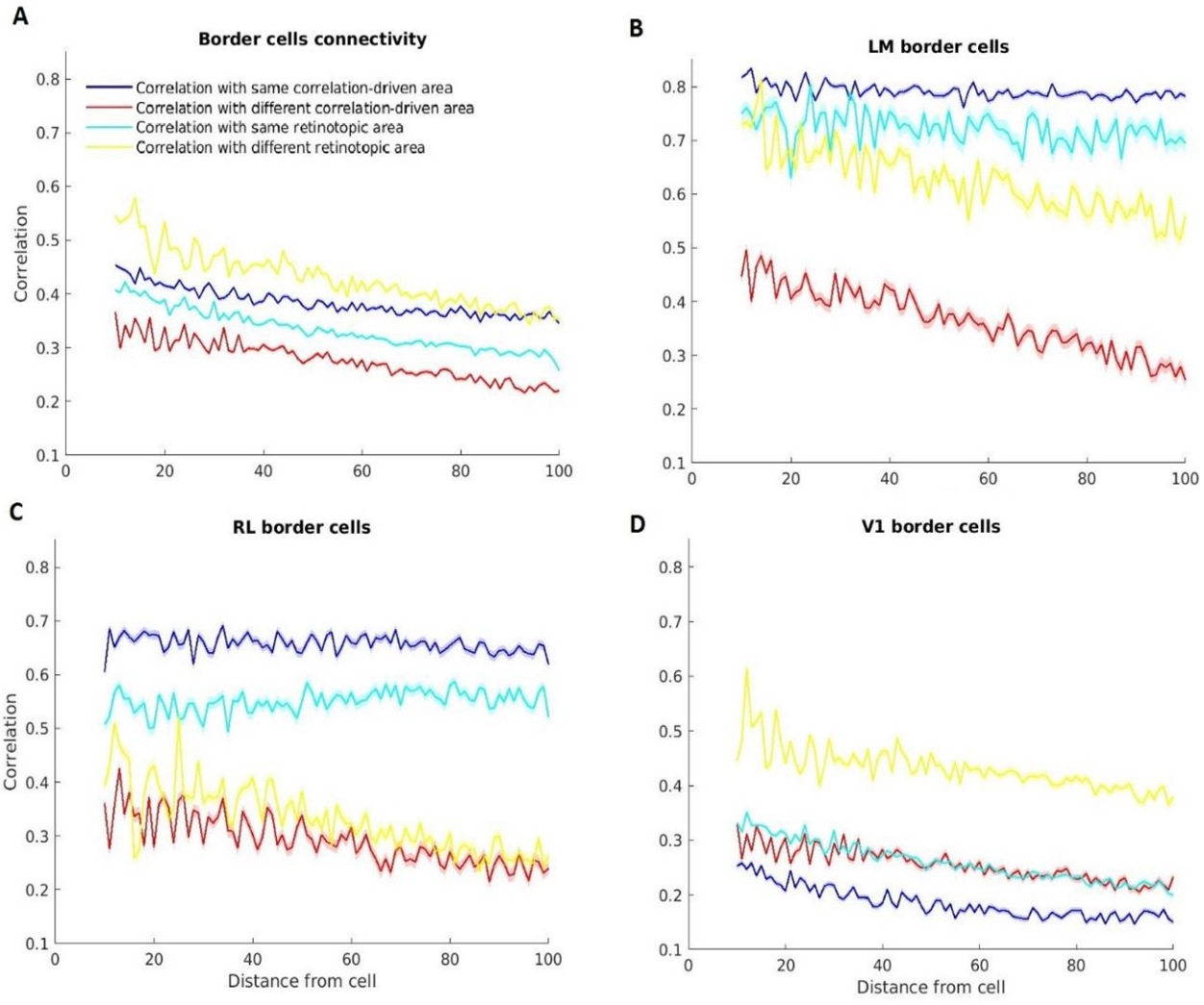
A
Border cells connectivity
Correlation with same correlation-driven area
Correlation with different correlation-driven area
Correlation with same retinotopic area
Correlation with different retinotopic area
Correlation
B
LM border cells
C
RL border cells
Correlation
Distance from cell
D
V1 border cells
Distance from cell

Figure 6. Border correlations within and across retinotopic and correlation-driven areas as a function of distance.

Correlations of border cells with identical and opposing labelling neurons exhibited higher divergence for correlation-driven organization compared to retinotopic arrangement. A, Correlation average of border cells with neurons of same correlation-driven label (blue), different correlation-driven label (red), same retinotopic mask (light blue), different retinotopic mask (yellow). Solid lines determine the mean, whereas transparent colors the standard errors. Distance is measured in μm. B, C, D, Same computations for each area separately. LM (B) and RL (C) correlations for cells within the same correlation-driven area are greater from interactions within the same retinotopic area. V1 (D), however, displays opposing patterns because of lower correlations to higher-order areas. This explains the eminence of inter-area correlations in reference to retinotopic organization in A. Distance measured in pixels (pixel = 2 x 2 μm).

Chapter 2.1.4 Correlation amplitude diminishes along the border

In order to further investigate neural correlations at the margins of visual areas, the interest focused on regions that include transitions from V1 cells to higher-order areas. The hypothesis was that correlation amplitude would operate in an inversed bell-shaped manner while crossing borders reaching its minimum at the novel correlation-established border. This is built on the basis that cells sharing identical labels have firmer connections from cell residing in opposing sides of the boundary.

To calculate the neural interactions along the border, correlations among cells were measured locally and organized in a matrix featured by the distance of each cell from border (Figure 7A, 7C). Each row of the matrix exhibits the unique interaction of a neuronal pair, measured as the Pearson's coefficient. The value of this computation is attributed to all the columns spanning the distance from the retinotopic border. This processing projected the spatial connections of

neurons to a line perpendicular to the retinotopic boundary. The size of the rectangle chosen for this operation was optimized for each analysis. Its rotation was adjusted to the orientation of the border and its length was assigned manually with the intention of involving cells both from center (training set) and border (testing set) of each area (Figure 7, top and bottom right), (see Methods).

Functional connectivity magnitude drops progressively when nearing the border (Figure 7B, 7D). It is very interesting that neurons within the border were anti-correlated. Hence, functional connectivity of cells could be used as a novel property for the identification of boundaries. Importantly, the corresponding location of the lowest point of correlation representing the connectivity-based border, demonstrated a shift relative to the retinotopic border. In addition, the displacement of the boundary agreed with the potential expansion of LM and RL into V1, identified in the map generated by NB predictions of the established model (Figure 2B).

Our initial assumption of an inversed bell-shaped mean correlation instead of a sharp-edged drop was motivated by the labeling ambiguity presented on the borders of the maps generated by the PCA+LDA algorithm. The estimation of correlations among neurons of conflicting classes within a territory of equivocation without sharp distinctions, lead to a broadened-shaped curve of mean correlation (Figure 7B, 7D). According to the neuronal correlations, a zone of vague area membership exists close to the borders. This findings align with the uncertainty occurring in the maps generated by the azimuth retinotopy (JH et al. 2011). Given that retinotopic maps are described by smooth reversals of retinotopic gradients, our findings could concur with the featured uncertainty of border delineation in Figure 1C, Figure 10 (Zhuang et al. 2017). Another observation that should be taken into consideration was that the width and sharpness of the correlation curve varied for the two borders examined. V1-RL boundary displayed a wider transition of the intensity of neural interactions, relative to V1-LM (Figure 7B, 7D).

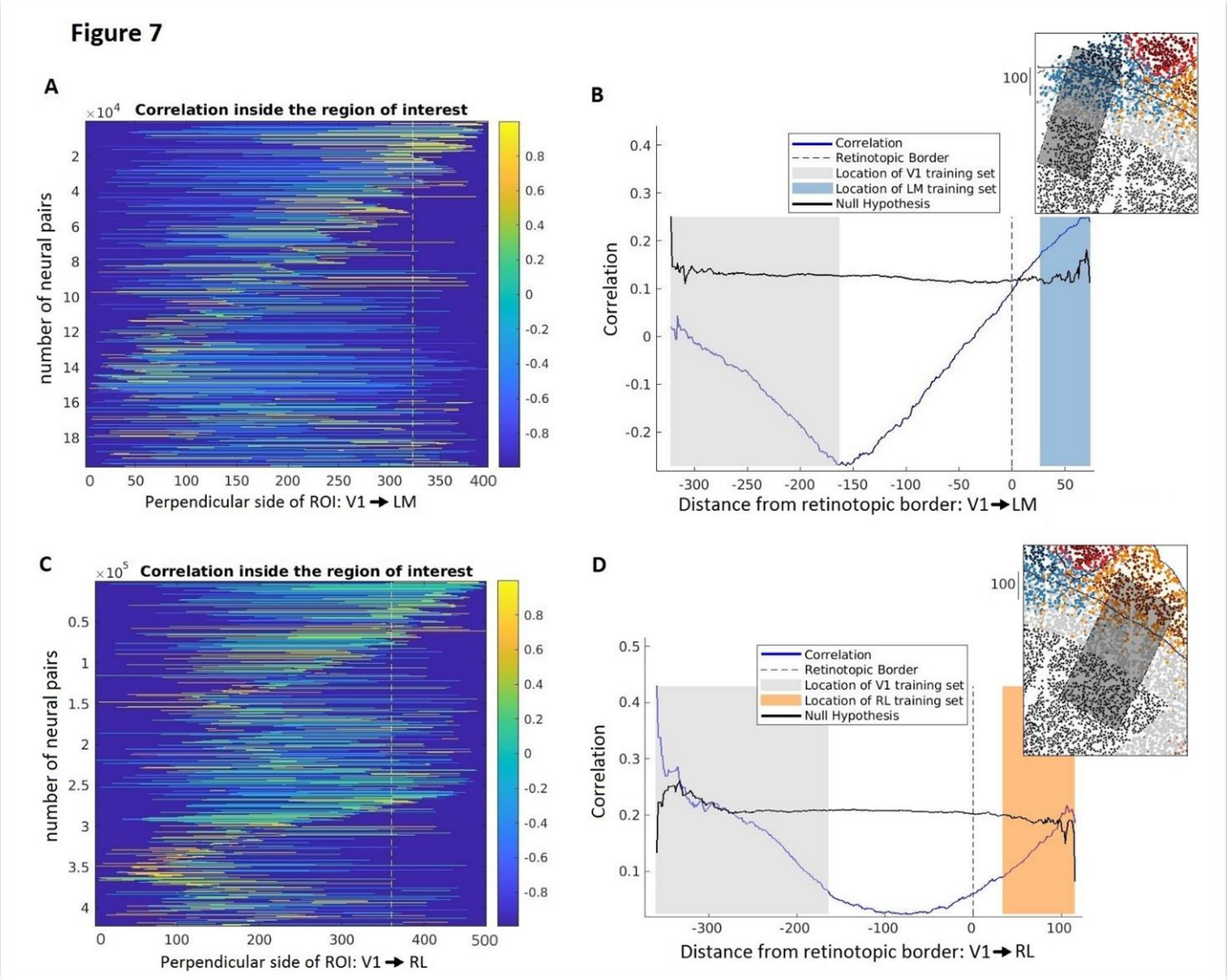

Figure 7. Correlations in transitions zones of V1 and high-order areas boundaries.

A, C, Matrix of neuronal pair correlations identified within the region of interest (ROI: A, V1-LM border, exhibited in top right. B, V1-RL border, bottom right) and determined by the distance of each cell from the boundary. Each row carries the value of correlation connecting the neuronal pair. The spectrum of colors determines the correlation amplitude. Vertical dotted line represents the location of the retinotopic border. B, D, Mean correlation (blue line) computed across all neuronal pairs. Black lines display the correlation average when neuronal pair correlations are randomized (see Methods). Background color defines the location of the training set for each area (LM: blue, RL: orange, V1: grey). Distance measured in pixels (pixel = 2 x 2 μm).

Chapter 2.1.5 Directionality of border cells corresponds to the center of visual areas

Additional computations were executed to gain a stronger insight into functional connectivity of cells residing near the border. For this purpose, directionality was introduced into the analysis (see Methods). Directionality of each cell was defined as the mean of a vector population (Figure 9A). Each connection of neuronal pair was determined by a complex number designating a vector in the Cartesian space. Correlation coefficient of a neuronal pair indicated the vector's amplitude while its angle defined their spatial relation into the scan. The number of vectors generated for each cell was equal to the number of pairwise connections. The distinct averaging of the real and imaginary part of the vector population resulted in a unique vector whose angle was representative of the cell preferred directionality (Figure 9A, red line). Since neural correlations diminished at the margins of neighboring visual areas, a plausible scenario would be that the preferred directionality of each border cell would point towards the center of the related area.

In order to provide a generalized visualization, the spatial layout of the preferred directionality for each cell is displayed for the borders of V1, LM, RL and AL. It is shown that the majority of cells in the borders points towards the center of the connectivity-based visual area (Figure 8). Concretely, the organization of the cell directionality within AL shapes a distinct pinwheel. Based on the structure of AL directionality arrangement the LM-AL and AL-RL retinotopic borders should be shifted towards AL and RL, respectively (Figure 8). Despite the potentials of the directionality to guide the delineation of visual cortex margins, the preferred neural orientations along the border were not necessarily as explicit as in the situation of AL. Specifically, the boundaries of V1 with LM and RL were defined by noisy orientations. While approaching the center of V1, neurons were described by an abrupt alteration of directionality. This is potentially the effect of LDA, as center cells, in contrast to neurons at the margins, had gained an insight into their class (see Methods).

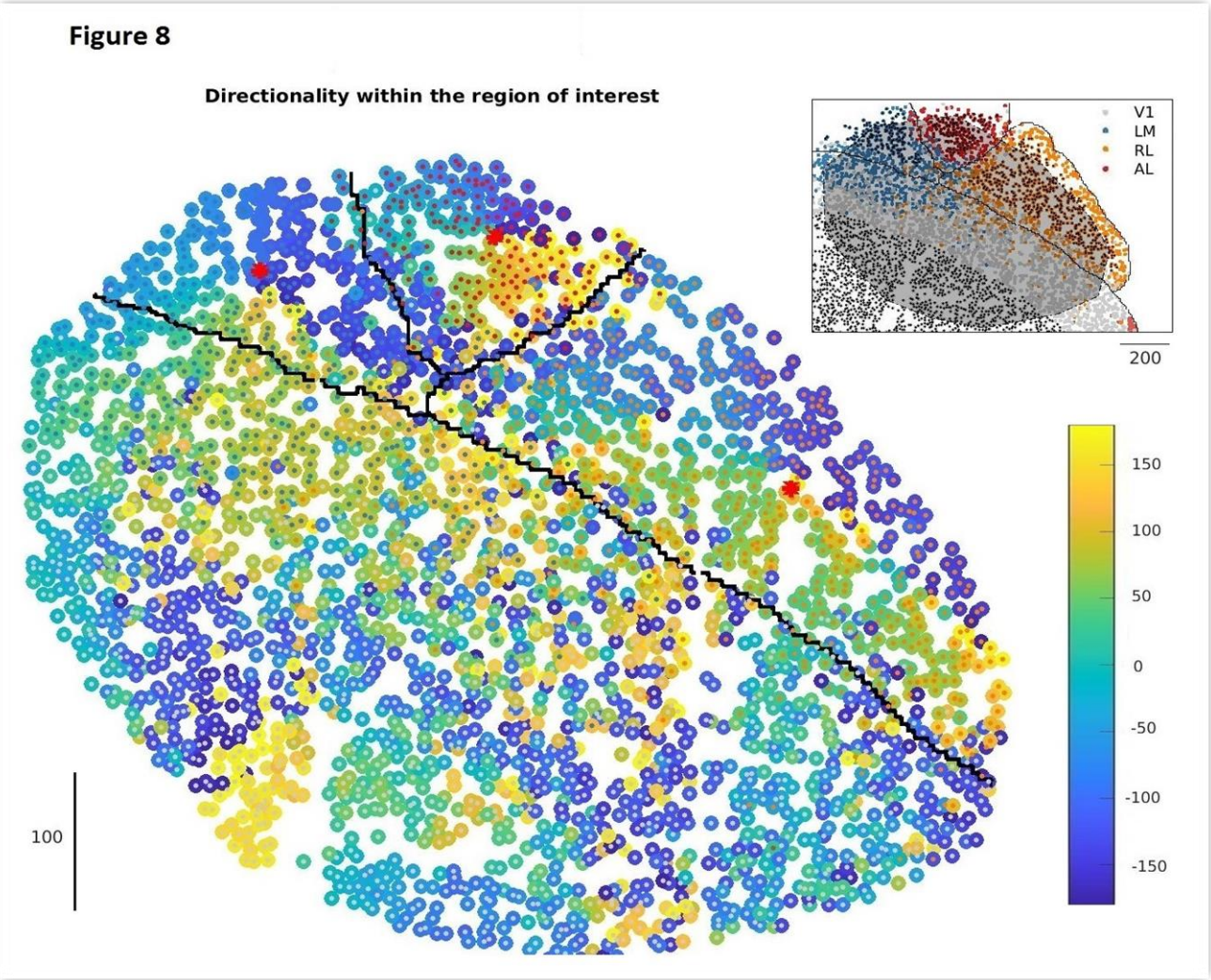

Figure 8. Spatial layout of directionality.

Each cell is displayed with two colors. The color spectrum (yellow to blue) represents the angle of preferred orientation for each cell, whereas the small dots within each cell determines the visual area based on the connectivity map. Top figure designates the region of interest. Cells close to the margins of visual areas tend to point towards the center of each area. Based on this pattern, LM tends to expand into V1 confirming the correlation driven-organization. Although directionality of cells nearby the boundaries of V1 to LM and RL are noisy, AL displays a pinwheel of cells oriented towards the centroid of the area.
Red asterisks represent the centroid of each area calculated based on the center cells. Distance measured in pixels (pixel = 2 x 2 µm).

To elucidate the noisy directionality identified along the V1 boundary, I focused on the transition from V1 to LM. The results provide evidence of a significant bimodal circular

distribution in the border of V1 with LM (Omnibus test; p-value < 0.01), with the preferred direction of connectivity pointing towards the corresponding areas (Figure 9B). It would be expected that cells assigned to LM based on the PCA+LDA algorithm should be defined by a directionality corresponding to the center of LM, i.e. [50 – 100] degrees, while V1 neurons should point to the center of V1, i.e. [-50 – -100] degrees. The labeling generated from the functional connectivity map, however, could not reflect the preferred connectivity orientation estimated for each cell. Therefore, although units were segmented into groups pointing to V1 and LM centroids, each cluster consisted of both V1 and LM neurons (Figure 9B).

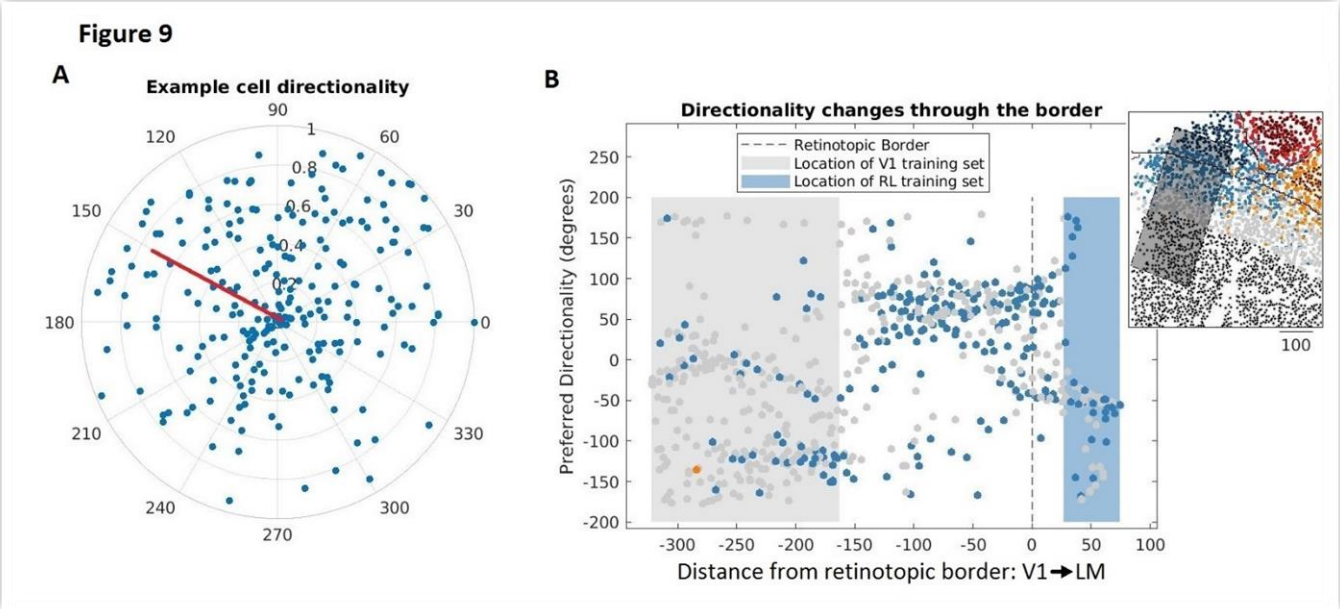

Figure 9. Directionality of cells within the region of interest identified at the V1-LM boundary.

Two subgroups of directionality identified in the LM-V1 border. A, Algorithm for the identification of the preferred correlation orientation an example neuron. Each dot represents a vector of neuronal connection for a particular neuronal pair. Amplitude is defined by the correlation coefficient and the angle represents the spatial relation of the neuronal pair within the scan. The red line determines the cell directionality computed by the average of the population vector. B, Directionality for the cells within the region of interest (right square). Background colors define the location of training neurons. Dotted vertical line represents the location of retinotopic border. The color of each dot designates the class of each cell according to the correlation-driven segmentation (LM: blue, V1: grey, RL: orange). Statistical significance for the bimodal circular distribution of cell directionality (Omnibus test; p-value < 0.01).

Chapter 2.1.6 The ambiguity of correlation-driven borders is verified by retinotopy

Functional connectivity indicated shifted boundaries relative to retinotopy and smooth transitions of correlations along the margins of visual cortex. In order to further investigate the discrepancy between the functional connectivity-based and retinotopic-based labeling near the borders, the afferent projections to visual areas were evaluated. It has been shown that both lateral posterior nucleus (LP) and lateral geniculate nucleus (LGN) of mouse thalamus are topographically organized with neurons that project to distinct visual areas (Juavinett et al. 2020). In particular, LP neurons mainly project to higher-order areas, while LGN to V1. Nonetheless, the anatomy of thalamo-cortical connections demonstrated spatially overlapping inputs in mouse visual cortex that probably generated retinotopic field coverage biases of higher-order areas (Juavinett et al. 2016), (Zhuang et al. 2017). Therefore, the spatial overlap of projections is evident through the interruption of the reversal of azimuth gradient by non-sequential values (Figure 10B). If this was the case, cells identified within the patch of V1 (Garrett et al. 2014) could have received input from LP neurons which carry information for higher-order areas.

The distribution of azimuth for cells within the patch of V1 close to borders were analyzed. According to the correlation-generated map, cells in this region were assigned to both LM and V1 (Figure 10A). It was expected that LM neurons within the V1 patch would exhibit roughly same values of azimuth with the margin values as potential outliers of the azimuth distribution of LM. On the other hand, V1 cells within the V1 patch would be more distant from the azimuth measured nearby the boundary. As a result, our assumption would be verified if the absolute differences of the azimuth for correlation-defined LM cells from the value of reversal at the margin were inferior to those computed for V1 neurons. Indeed, our estimation was valid as LM cells had significant divergence from the V1 distribution (Figure 10C). This distinction confirms the spatial overlap displayed in previous studies (Juavinett et al. 2020). Moreover, the findings designate the correlation-driven organization of visual areas as a reliable arrangement, which might be partially explained by projections of thalamic nuclei.

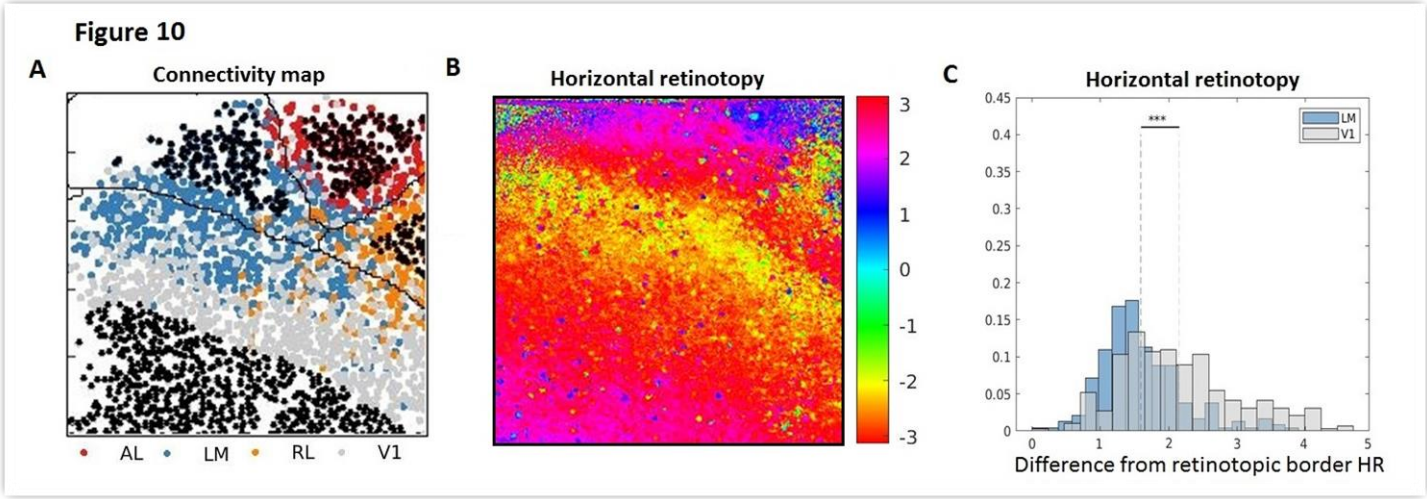

Figure 10. Interruption of smooth progression of azimuth identified in V1-LM border by LM cells penetrating the V1 patch.

LM neurons penetrating V1 patch display horizontal retinotopy similar to the azimuth attributed to the boundary. A, Connectivity-based segmentation of V1 (grey), LM (blue), RL (orange) and AL (red). B, Horizontal retinotopy transition through the border of V1-LM. Degrees in radians. C, Histograms of horizontal retinotopy difference from values attributed to the boundary for LM (blue) and V1 (grey). Statistical significance: t-test, p-value < 0.01. Higher values represent less proximity to the azimuth of the boundary and, therefore, the distribution of LM. HR: Horizontal Retinotopy.

Chapter 2.1.7 Functional connectivity map generated by presentations of objects

In previous sections, a connectivity map originated by the neuronal responses of mice to the presentation of movie specified by wealthy spatiotemporal statistics was established (Field 1987), (Esfahany et al. 2018). Stimuli consisted of movie clips that were extracted from “Mad Max” and “Matrix”. Here, moving objects were employed as a stimulus for the construction of a functional connectivity map. Therefore, these movies might substantially affect neural responses through retinotopy, as their unfolding produce the activation of neuronal assemblies with receptive fields corresponding to the location of the moving object.

The network was structured in a manner resembling the map produced earlier from typical movies (Figure 11A). Correlations within areas were enough for generating a potential connectivity map that would correspond to the retinotopic borders. The displacement of the V1-LM borders was, in fact, greater than the shift observed at the connectivity map originated by previous movies (Figure 2B). Within versus across area connectivity exhibited statistically significant differences for both computations employed before and after the PCA+LDA algorithm (Figure 11B, 11C). Specifically, the statistical power of divergence was amplified after the application of our model (Figure 11B, 11C, F-statistic).

Therefore, correlations are possibly not affected by the identity of the stimulus as long as the presentation fits the criteria for effectively activating neurons (Kayser, Körding, and König 2004). These findings conflicted with the nature of measuring ‘noise’. Considering that ‘noise’ is calculated as the deviation from the stimulus-driven response, it is reasonable to expect that ‘noise’ correlations are dependent to the features of the movie (Vinje and Gallant 2000). However, the results implied a dissociation of noise with bottom-up coding (Merrikhi, Clark, and Noudoost 2018), as the connectivity maps generated by the presentation of movies and objects displayed many similarities.

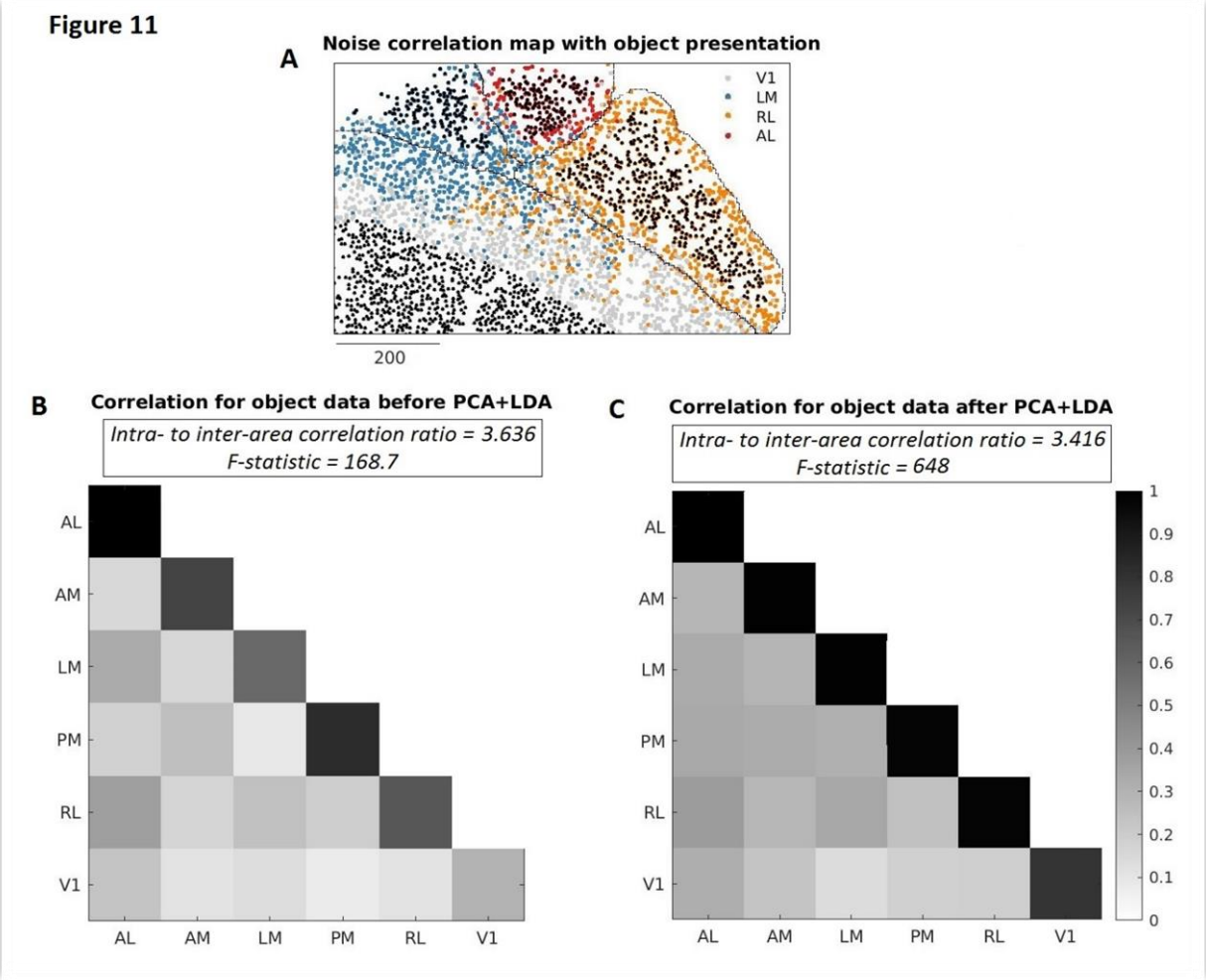

Figure 11. 'Noise' connectivity map with object presentation.

Correlation-driven map generated from presentations of movies with moving objects exhibited great resemblance to connectivity map originated from presentation of complex movies. A, Connectivity map originated from trials with presentation of movies with moving objects. B, C, Correlations before (left) and after PCA+LDA (right). Statistical significance among the intra- and inter-area correlations for all scans (ANOVA: p-value < 0.01). The mean correlation matrix is normalized between 0 and 1, in both cases. Inter- to intra-area correlation ratio was slightly reduced, while F-statistic was amplified after the PCA+LDA algorithm. Black bar describes the size of the scan in pixels (pixel = 2 x 2 μm).

Chapter 2.1.8 Functional connectivity map generated by spontaneous data

In order to discover the origins of 'noise' correlations, the same procedure was performed for data obtained from time periods without stimulus, when a grey screen was present. Theoretically, spontaneous data represents both the bottom-up projections and internal factors that modify neural activity (Gilbert and Li 2013). The organization of visual cortex according to spontaneous activity exhibited essential resemblance with the two maps generated in previous sections (Figure 2B, Figure 11A, Figure 12A). Intra-area correlations induced by spontaneous activity were significantly higher from inter-area correlations (Figure 12B, 12C). Importantly, the distinction among the two groups augmented after the application of PCA+LDA algorithm. Even so, it seemed like the membership of border cells was designated by non-negligible ambiguity. In fact, spontaneous correlations demonstrated an arrangement of V1-LM border that was a mixture of 'noise' and 'signal' connectivity map (Figure 2).

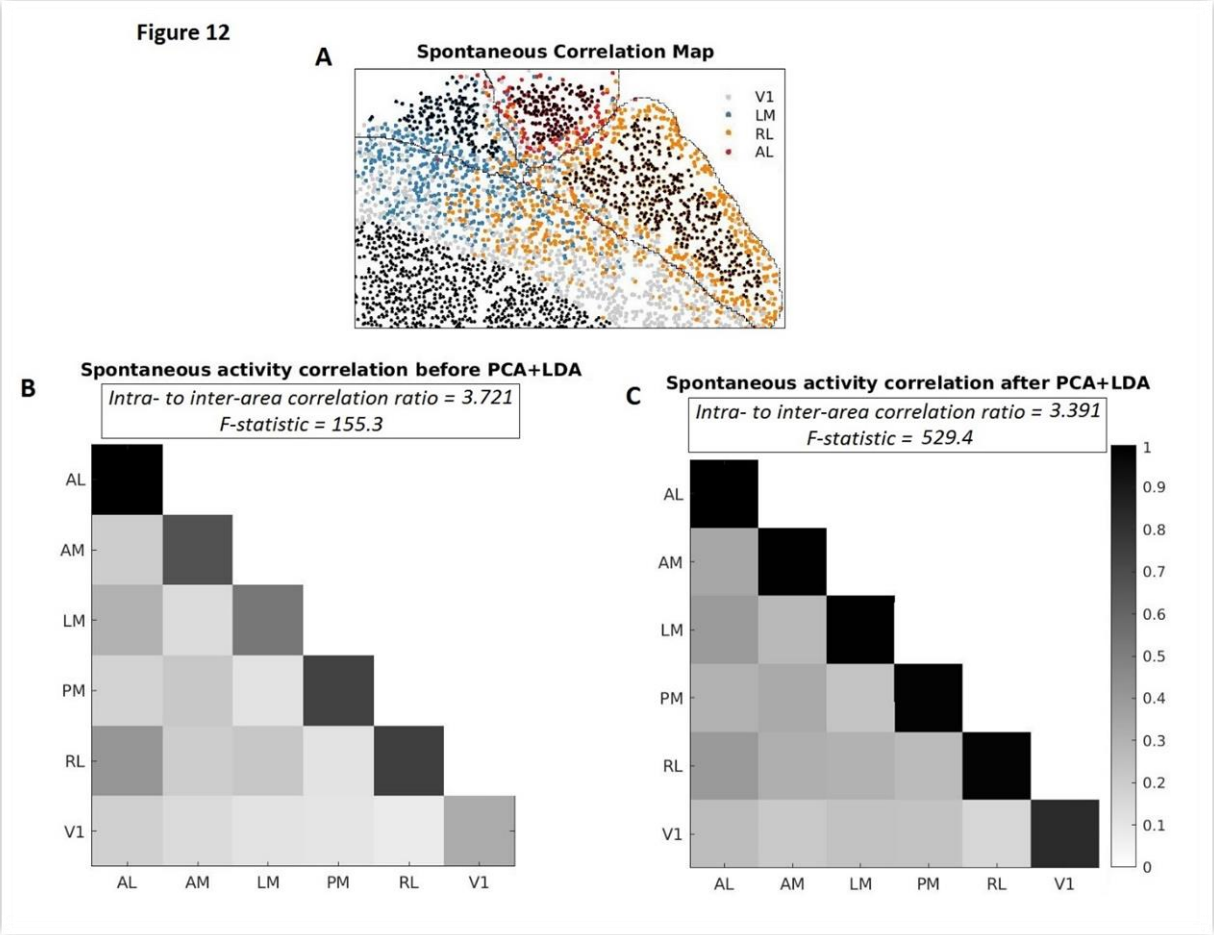

Figure 12. Spontaneous connectivity map.

Correlation-driven map generated from spontaneous activity exhibited important similarities with the retinotopic. A, Connectivity map originated from periods without stimulation (grey screen). B, C, Spontaneous correlations before (left) and after PCA+LDA (right). Statistical significance among the intra- and inter-area correlations for all scans (ANOVA: p-value < 0.01). The mean correlation matrix is normalized between 0 and 1, in both cases. The statistical power of divergence among within and across area correlations increased after the application of PCA+LDA (F-statistics in B and C). Black bar describes the size of the scan in pixels (pixel = 2 x 2 μm).

Chapter 2.2 Assignment of visual area boundaries mediated by complementary functional parameters

Additional neural parameters were investigated with the expectation of co-aligning to the organization of visual cortex assessed by functional connectivity. For this purpose, the initial goal was to identify properties that were discriminated across visual areas. In case of substantial discrepancy, an attempt was made for evaluating the label of each border cell. The probability of a neuron to belong to the retinotopic or the correlation-driven area was quantified through the computation of the likelihood based on the probability density functions of the functional parameters. For example, if a cell was residing within the V1 patch and the algorithm classified it to LM, it was important to assess its true label according to the probability measured by the distributions of the functional parameter for the two opposing visual areas. In the same direction, a Receiver Operating Characteristic (ROC) Analysis enabled the estimation of the performance of the functional parameter to distinguish the border cells of neighboring visual areas by taking into account the functional connectivity- or the retintopy-based arrangement.

Variable functional properties were examined in order to identify significant divisions among the visual areas. The decoding performance of each cell to predict the identity of the stimulus (Froudarakis et al. 2020), the selectivity to the optic flow of the movie (Patel and Upadhyay 2013) and the signal-to-noise ratio of the receptive field (Froudarakis et al. 2020) constitute few of the attempts. However, only the reliability (Froudarakis et al. 2020), the state dependence (Ecker et al. 2014) and the response decay timescale (Siegle et al. 2021) displayed interesting results.

Chapter 2.2.1 Reliability agrees with the correlation-driven topographic expansion of LM

Our initial question was how neurons respond to repeated stimuli. It is well known that neuronal reponses are highly variable to the presentation of identical stimuli (Heggelund and Albus 1978), (Doiron et al. 2016). However, the origin and nature of trial-to-trial variability are poorly understood.

If fluctuations of neural activity depend on the cortical states and there is differential effect of the states to different cortical regions, then a metric that quantifies the variability could be utilized in order to distinguish the identity of border cells (Gur and Snodderly 2006). This metric is the reliability which is measured as the ratio of true variance (i.e. variance produced by stimulus) to the total variance (i.e. variance caused by 'signal' and 'noise'). Therefore, reliability was calculated by dividing the variance of the stimulus-driven responses by the total variance of the activity of each cell.

Data obtained from an example session exhibited important divergence among V1, LM and RL distributions of reliability (Figure 13A-13D). As a result, reliability could be a potential discriminating property for V1 and higher-order areas. An exciting observation was that correlation-defined border cells exhibited similar ROC curve shapes with the center cells, while comparing functional connectivity to retinotopic arrangement in V1-LM border (Figure 13E). Contrariwise, this could not be detected while operating in the context of V1-RL border, as the diagnostic ability of the retinotopic and connectivity-based border configuration were indistinguishable (Figure 13F, red and green line). Nonetheless, this might be the result of the important similarities identified between the functional and retinotopic organizations of V1-RL boundary (Figure 13A).

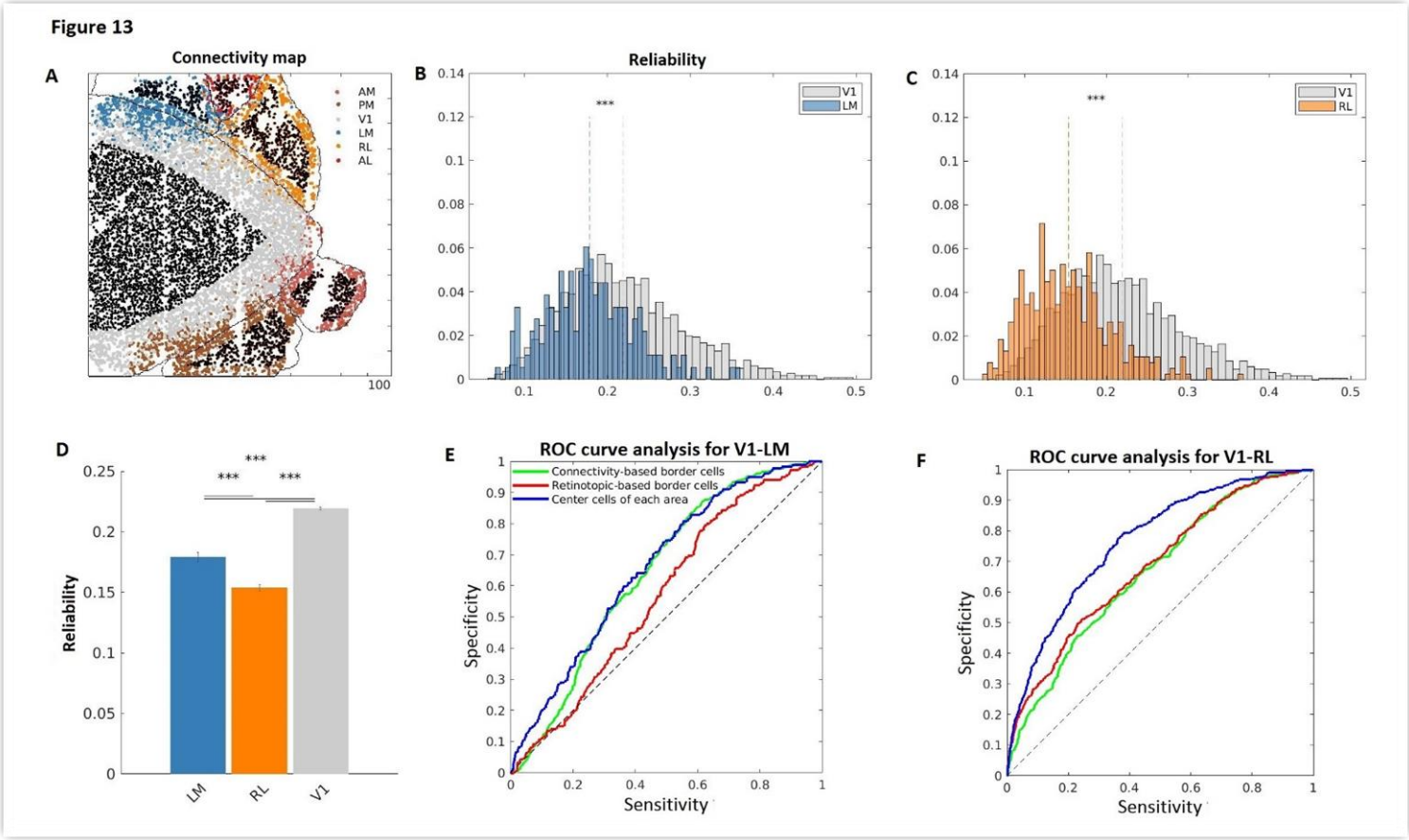

Figure 13. Comparison of the retinotopic and correlation-driven organization at the borders in reference to reliability.

Reliability could be used to discriminate border cells in a manner corresponding to connectivity for LM-V1 border. A, Connectivity map of example scan. B, C, Reliability histograms of visual areas for an example session (t-test: p-values < 0.01 for both LM and RL divergence from V1, in B and C, respectively). D, Mean reliability and standard error for V1, LM and RL. A statistical significance between the three areas was identified (ANOVA: p-value < 0.01). For all the calculations of each area, only the center cells were accounted in order to minimize the influence of retinotopically defined areas. E, F, ROC analysis computed for center cells (blue line), border cells defined by connectivity (green line) or retinotopy (red line) in order to identify discriminations within the V1-LM (E) and V1-RL (F) margins. LM and RL represent the positive class, whereas V1 the negative for the calculation of sensitivity and

In order to further analyze a potential organization deriving from reliability, the spatial arrangement of reliability in a region adjacent to the borders of V1, LM and RL was assessed (Figure 14). A map was generated in order to display the distance from the "criterion" identified at the intersection point of the center cell distributions of the correlation- and retinotopic-attributed areas of each cell. Positive values of distance designated a correct assignment of cells according to functional connectivity, while color intensity determined the level of confidence (see Methods). As a consequence, 'green' neurons illustrated cells with greater chance to belong into the correlation-emerged classes, while 'purple' neurons were related to a higher degree with their retinotopic class (Figure 14). Even though the magnitude of distance from criterion were weak, the modulation of margins in reference to reliability coincide with the connectivity-based expansion of LM at the expense of the V1 extent, as most cells assigned to LM within the V1 patch had higher possibility to belong to LM. On the other hand, the segmentation of V1 to RL and, also, boundaries within higher-order areas were associated with the retinotopic arrangement (Figure 14). Concretely, cells assigned to RL, according to the PCA+LDA algorithm, located within V1 were in majority falsely labelled.

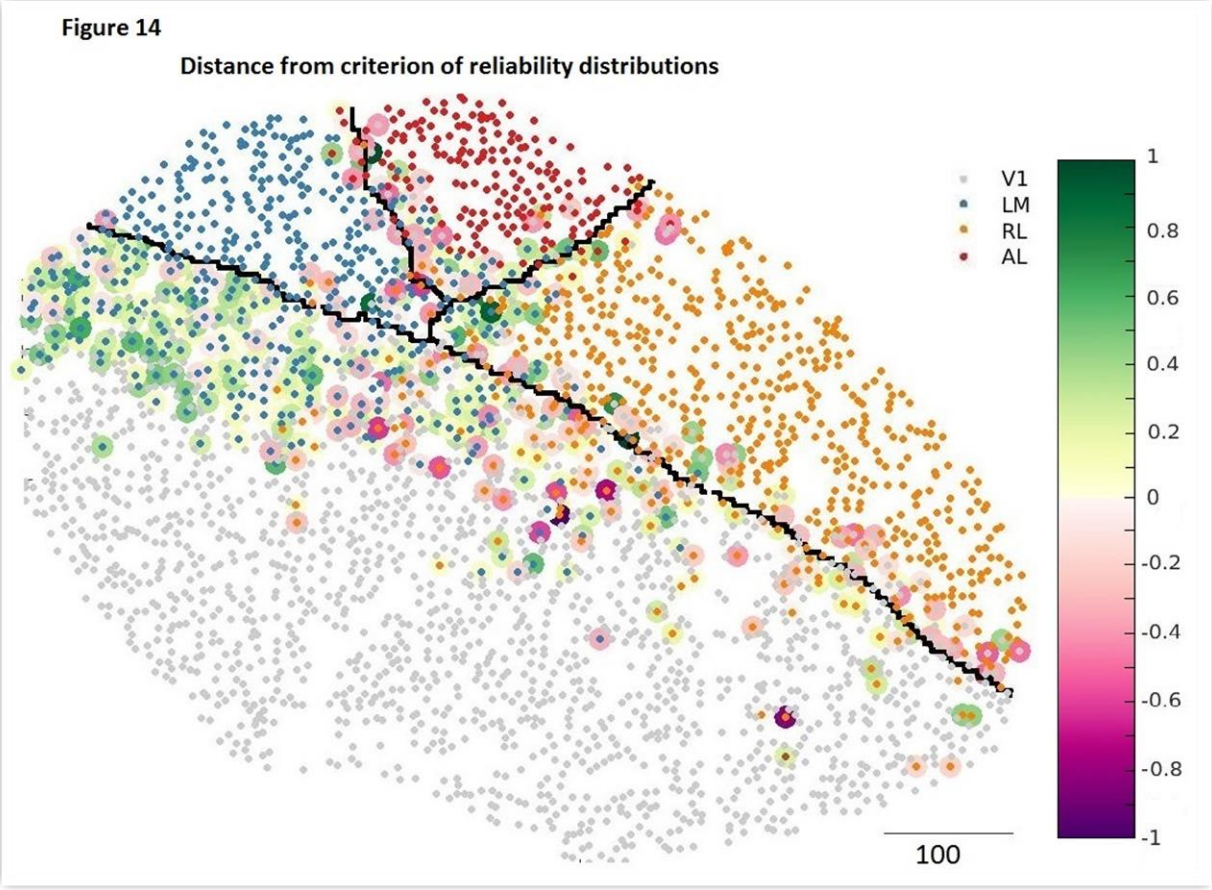

Figure 14. Spatial layout of distance from “criterion” defined by reliability distributions for border cells with opposing labels according to retinotopy and connectivity.

V1-LM border organization based on reliability agrees with the connectivity expansion of LM over V1. The bars of ‘yellow to green’ and ‘pink to purple’ determine the distance from the intersection point of retinotopic and correlation-driven area distributions. Cells with values from -1 to 0 (purple range dots) represent neurons that did not align to the organization structure of connectivity map, whereas cells within the yellow-green spectrum (i.e. from 0 to 1) concur with the connectivity map. The smaller dots designate the label predicted from NB classifier according to the model generated (V1: grey, RL: orange, LM: blue, AL: red). Black bar describes the size of the region in pixels (pixel = 2 x 2 µm).

Next, an effort was made to characterize the reliability across different recordings. V1 displayed greater reliability compared to higher-order areas (Figure 15A, 15B). ROC curve analysis underlined the eminence of reliability to discriminate V1-LM border cells when neural labels were indicative of the connectivity layout rather than the retinotopic (Figure 15C). On the other hand, V1-RL border was better explained by the retinotopic topography (Figure 15D). AUCs of all ROC curves of every scan for V1-LM and V1-RL reliability distributions were discriminated with statistical significance in favor to connectivity and retinotopic configurations, respectively (Figure 15E, 15F).

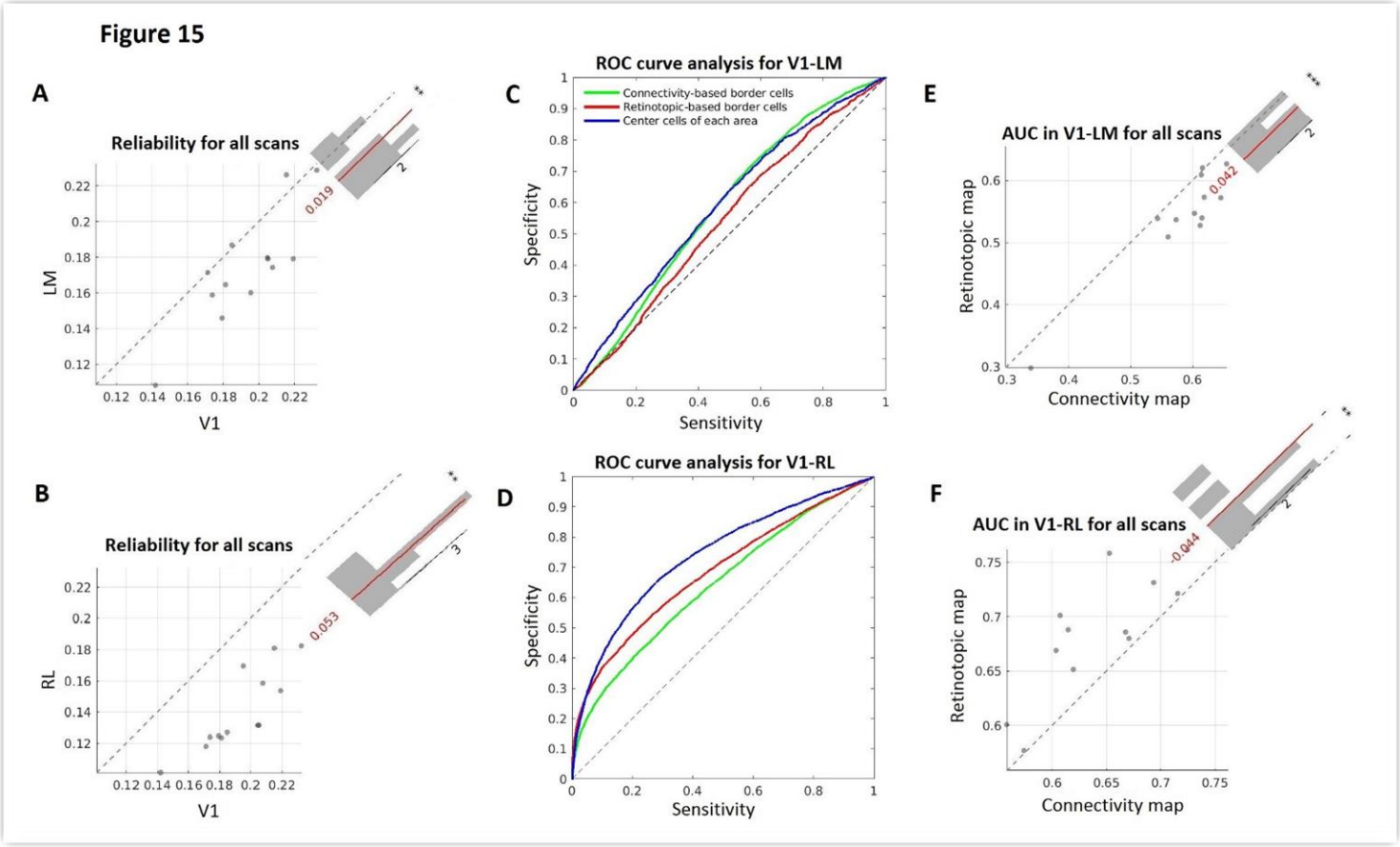

Figure 15. Evaluation of V1-LM and V1-RL discrimination in reference to the border cell reliability for all scans.

The organization of reliability at the V1-LM boundary concur with the connectivity configuration. A, B, V1 exhibit significantly higher reliability compared to higher-order areas (t-test: p-value < 0.05). C, D, ROC curves for the comparison of the correlation-driven segmentation of border cells (green line), the retinotopic arrangement of borders (red line) and the center cells of each area (blue line). Reliability assigns V1-LM border cells with higher performance when computed for the correlation-driven labels (green line superior to red). E, AUCs of connectivity-based computations of reliability over all scans display a statistically significant difference from the retinotopic arrangement (t-test: p-value < 0.01). F, The converse applies for the AUC analysis of V1-RL borders, as the retinotopic configuration of reliability in V1-RL border outperforms the connectivity ROC curve (D), (t-test: p-value < 0.05).

Chapter 2.2.2 Borders are organized based on differentiating dependencies of neural activity to the animal state

As previously mentioned, neuronal responses elicited by presentations of identical stimuli show significant 'noise' correlations. Neural networks exhibit variable states that modulate the fluctuations of neural activity (Sherman and Guillery 1998), (Ecker et al. 2014), an association generated mainly by top-down regulations (Cohen and Newsome 2008). Hence, a question is how cognitive states, and particularly arousal in our case, affect 'noise' correlations which were proposed earlier as a discrimination property of visual areas. The state-dependence for each neuron was measured as the difference among the average firing rate of each cell for the active and quiet state normalized by their sum (see Methods). The separation rule for the two states of the mouse were determined by placing a threshold at the velocity of the treadmill where the task was performed (Supplementary Figure 1).

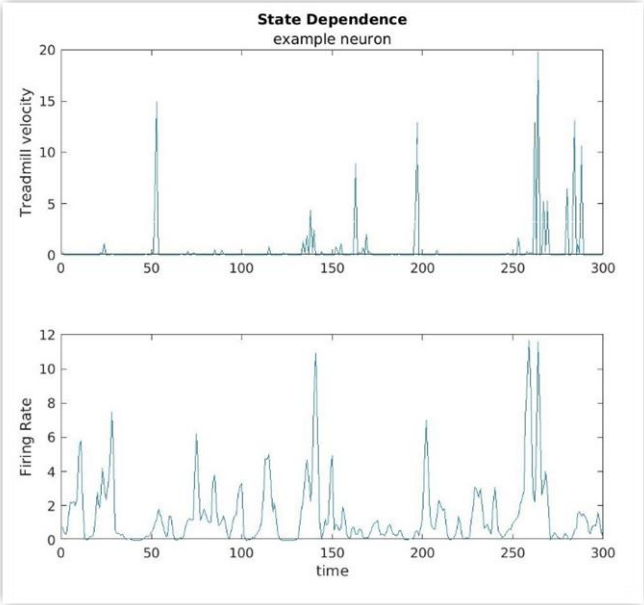

Supplementary Figure 1. Computation of State Dependence

Top: the treadmill velocity for a random trial (duration = 10s, sampling = 30Hz). Bottom: activity of an example V1 neuron during the trial. A threshold was placed for the treadmill velocity dividing the state of mouse in active and quiet state (see Methods). The ratio of the difference to the sum of the average neural activity for each state measures the dependence of each area.

For an example scan, the computation of the normalized distribution displayed a statistically significant difference among V1 and the higher-order areas (Figure 16A-16C). Although V1 exhibited a positive dependence to the arousal of the mouse, the mean firing rate of cells within

LM and RL during the quiet state of the mouse was greater compared to the active state (Figure 16D). In addition, the ROC analysis provided evidence for a better segregation of state dependence distributions of border cells when they were defined by the correlation-driven organization relative to the retinotopic arrangement (Figure 16E, 16F, green and red line). These findings corresponded both for V1-LM and V1-RL border. It is important to mention that the configuration of border cells by connectivity outperformed the discriminability of the state dependence distributions of center cells among V1 and LM (Figure 16E, green and blue line).

Figure 16

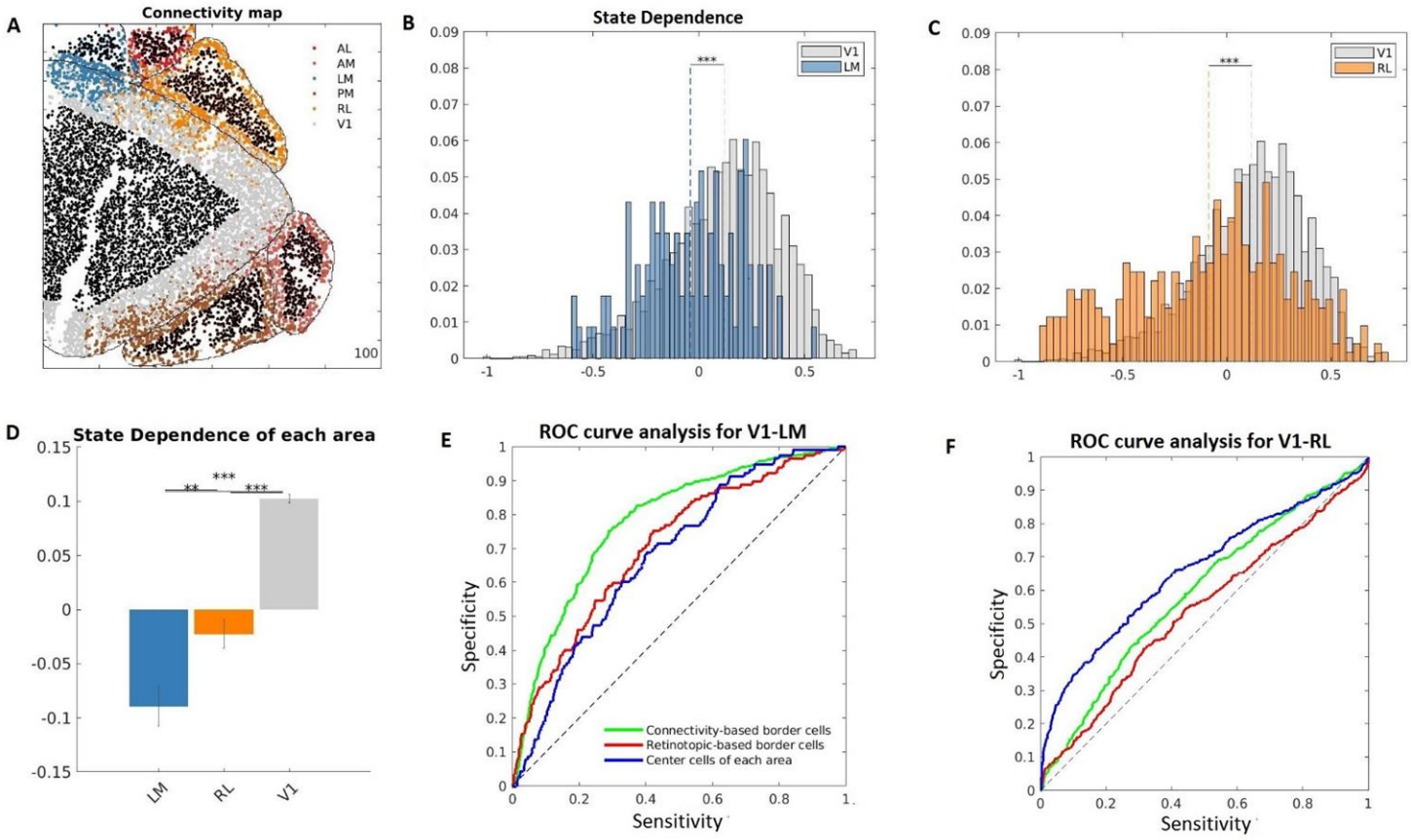

Figure 16. Differing dependence of each area from the mouse state.

A, Connectivity map of an example scan. B, C, Normalized probability distributions of the state dependence metric for LM (B) and RL (C), (t-test: p-value < 0.01). D, Mean values and standard errors of state dependence for LM, RL and V1 (ANOVA: p-value < 0.01). E, F, ROC analysis computed for center cells (blue line), border cells defined by connectivity (green line) or retinotopy (red line) in order to identify discriminations within the V1-LM (E) and V1-RL (F) margins. LM and RL represent the positive class, whereas V1 the negative class for the calculation of sensitivity and specificity.

In order to provide a visualization of the association between connectivity and the configuration of borders according to the state dependence, the analysis focused on a small area that includes many borders in one scan (Figure 17). It is demonstrated that state dependence designates V1-LM border in a similar manner to connectivity. Moreover, cells within the AL patch assigned to LM based on correlations, had higher likelihood to belong to AL.

State dependence of V1 cells penetrating RL was closer to the distribution of their correlation-derived label. The opposite pattern is observed with the cells attributed to RL within the V1 patch. It appeared as if the topographic configuration of the boundaries according to state dependence disputed the correlation-driven assignment of neurons to RL which were importantly distant from RL patch.

Therefore, the RL neurons within the V1 patch were controversial and could potentially constitute invalid predictions of our model. The opposite effect is highlighted for the LM neurons penetrating the V1 patch. Consequently, considering the entire functional entity of cells, the margins of V1 with the higher-order areas seemed to delineate a V1-LM border favoring the expansion of LM, whereas V1-RL border tended to approximate the retinotopic boundary.

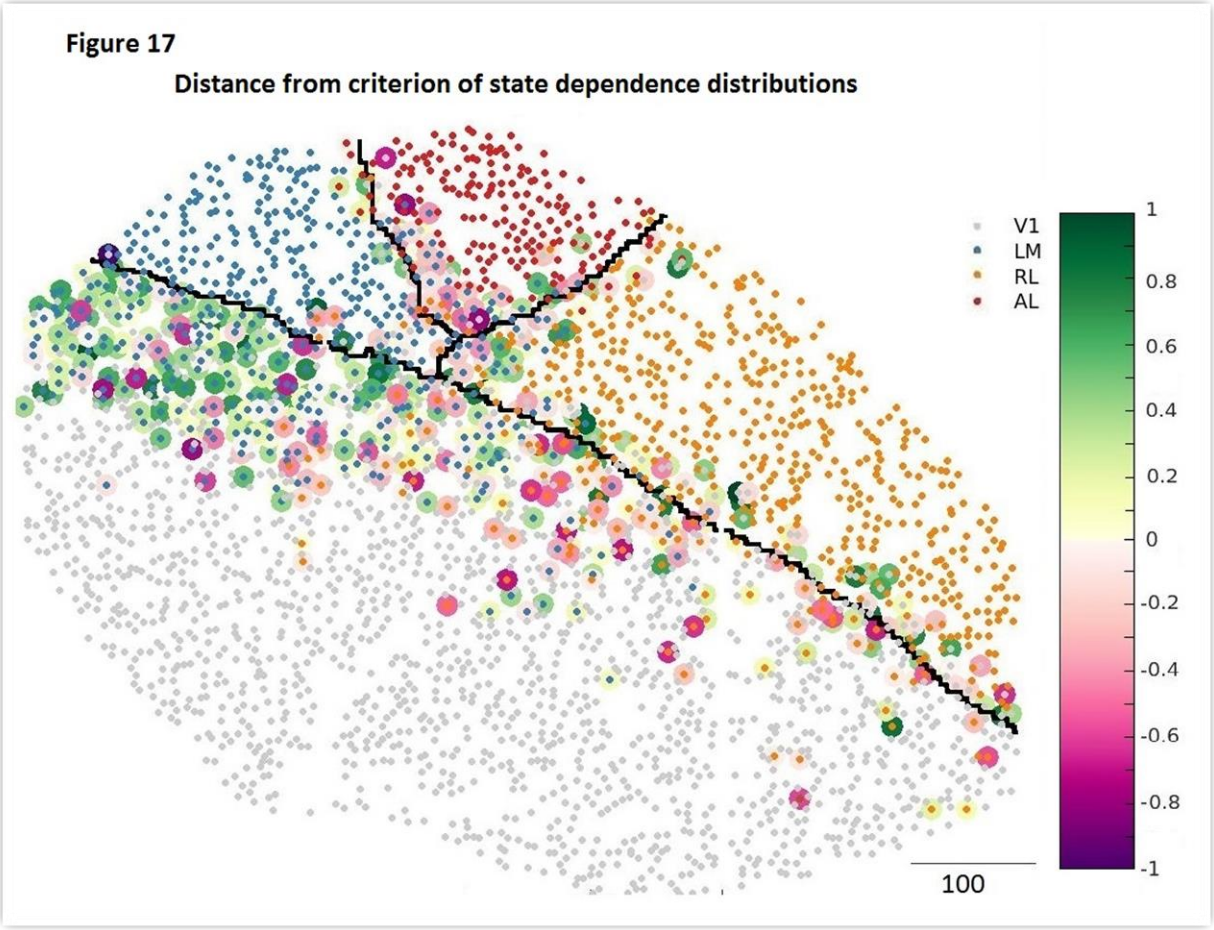

Figure 17. Spatial layout of distance from “criterion” defined by state dependence probability distributions for border cells with opposing labels according to retinotopy and connectivity.

V1-LM border organization based on state dependence agrees up to a point with the connectivity expansion of LM over V1 and the restriction of RL at the V1-RL boundary. The bars of ‘yellow to green’ and ‘pink to purple’ determine the distance from the intersection point of retinotopic and correlation-driven area distributions. Cells with values from -1 to 0 (purple range dots) represent neurons that did not align with the organization structure of connectivity map, whereas cells within the yellow-green spectrum (i.e. from 0 to 1) concur with the connectivity map. The smaller dots determine the label predicted from NB classifier according to the model generated (V1: grey, RL: orange, LM: blue, AL: red). Black bar describes the size of the region in pixels (pixel = 2 x 2 µm).

The extension of the analysis across all scans demonstrated consistent differences among V1 and higher-order areas, particularly for RL (Figure 18A, 18B). The averaged ROC curves for V1-LM and V1-RL discrimination identified slight divergence among the connectivity and retinotopic arrangement, with correlation-defined segmentation outperforming the retinotopic in both situations (Figure 18C, 18D). Despite the above, AUC analysis across all scans could not identify any significant differences (Figure 18E, 18F).

Figure 18

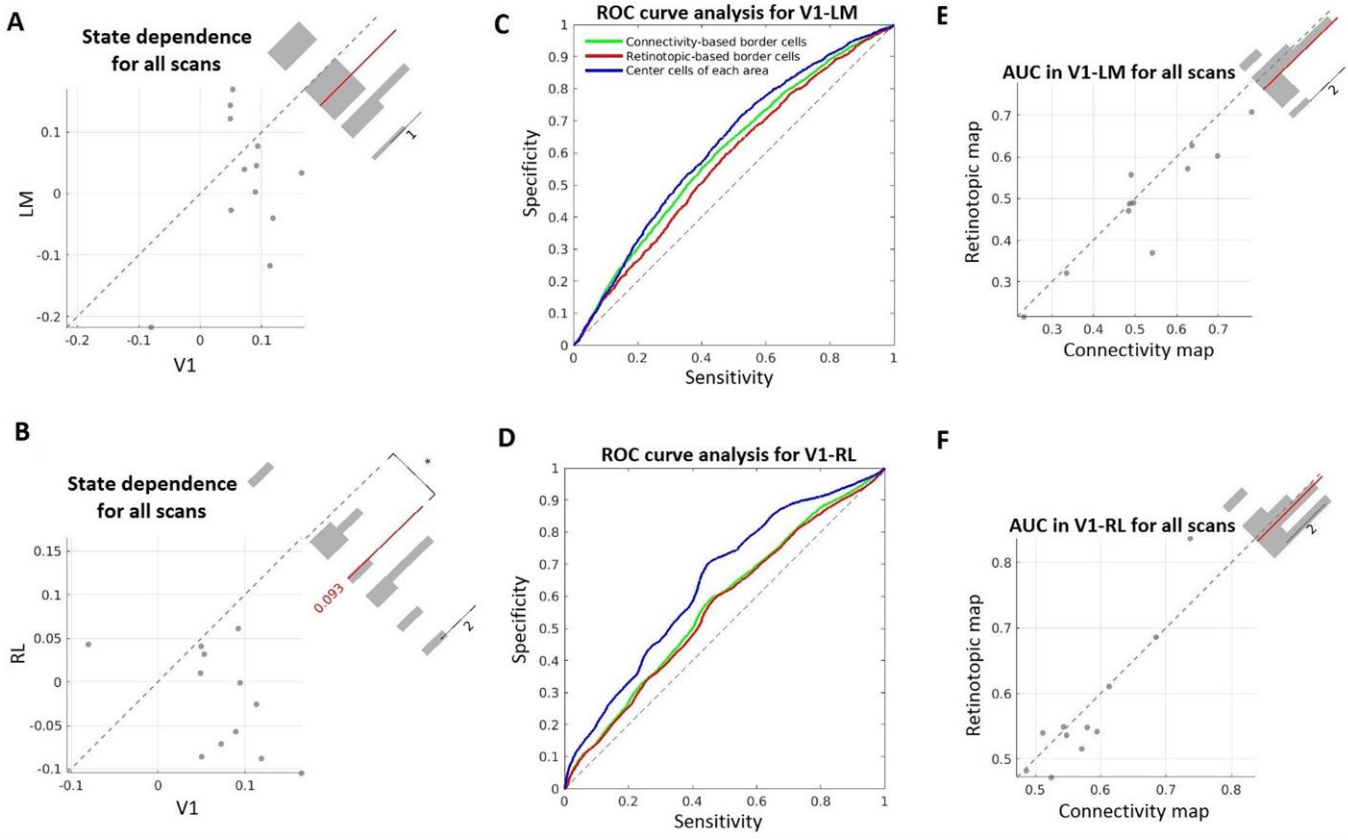

Figure 18. Estimation of V1-LM and V1-RL discrimination in reference to the state dependence of border cells for all scans.

The organization of state dependence at the V1-LM and V1-RL boundary concur with the connectivity configuration. A, B, V1 neurons exhibited higher firing rate during the active state across for all scans, in contrast to LM and RL (t-test: p-value < 0.1 for V1-RL, no statistical difference for V1-LM). C, D, ROC curves for the comparison of the correlation-driven segmentation of border cells (green line), the retinotopic arrangement of borders (red line) and the center cells of each area (blue line). State dependence neural activity discrimination of border cells performed in a similar manner both for the retinotopic and correlation-driven organization (green line superior to red, for both V1-LM (C) and V1-RL (D) margins), AUC over all scans could not identify a statistically significant difference from the retinotopic arrangement neither for V1-LM (E) or V1-RL (F) ROC curves (t-test).

Chapter 2.2.3 Response decay timescale agrees with the correlation-driven topographic arrangement of LM

Previous studies have indicated that the temporal stability of neural representation increases along the visual hierarchy (Piasini et al. 2021). These findings were attributed to the temporal broadening of neuronal receptive fields and the impact of intrinsic dynamics. Therefore, an attempt was made to evaluate the autocorrelation timescale of each cell (Siegle et al. 2021). Autocorrelation was estimated for each unit during the presentation of movies. After the autocorrelation curve was fit to an exponential decay function, the time constant was computed for each neuron (Supplementary figure 2, see Methods).

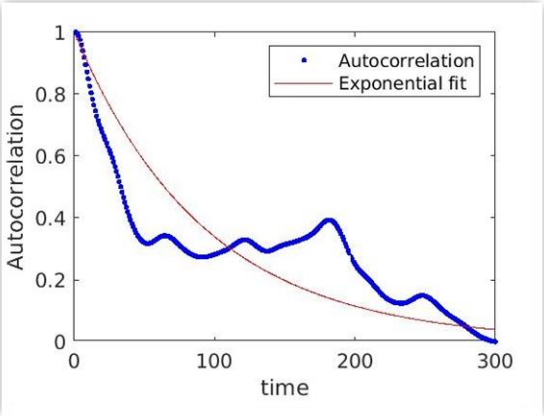

Supplementary figure 2. Response decay timescale calculation for each cell
Computation of autocorrelation (blue dots) and curve fitting to an exponential decay function (red line) for an example cell. The response decay timescale is calculated as the decay time constant describing the fitting function (red line).

Data obtained from an example session, displayed significant divergence for the response decay timescale of V1, LM and RL distributions (Figure 19A-19D). Therefore, higher-order areas maintain stimulus-evoked activity over longer temporal windows. This might complement the broadening of receptive field sizes along the visual hierarchy (Lennie 1998). ROC curve analysis underlined the superiority of the connectivity arrangement within V1-LM boundary for segregating cells in reference to the distributions of response timescale (Figure 19E). Nonetheless, neurons' timescales divergence for each area was not always harmonized with the correlation-

based topography. In fact, the association of the temporal dynamics with the NB predicted labels at the V1-RL boundary was inferior to the retinotopic modulation (Figure 19F).

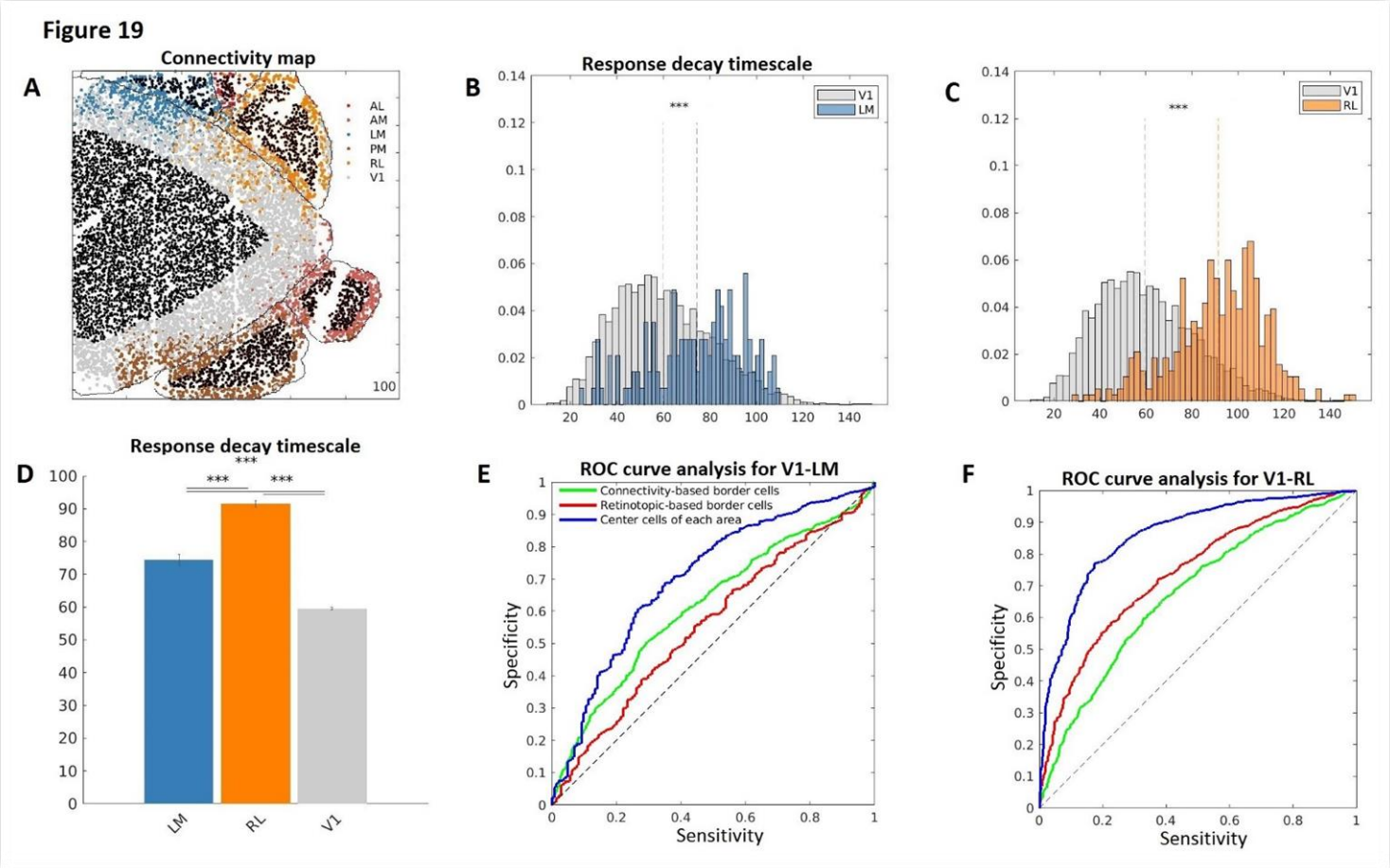

Figure 19. Discrimination of border cells in reference to response decay timescale.

Correlation-driven arrangement of V1-LM border provided better separating performance of response timescale compared to retinotopy. The situation conversed in V1-RL border organization. A, Connectivity map of example scan. B, C, Probability distributions of response decay timescale for V1 and higher-order areas (LM, RL). Statistical significant difference is detected with t-test (p-value < 0.01). D, Comparison of all areas of interest (ANOVA: p-value < 0.01). E, F, ROC analysis computed for center cells (blue line), border cells defined by connectivity (green line) or retinotopy (red line) in order to identify discriminations within the V1-LM (E) and V1-RL (F) margins. LM and RL represent the positive class, whereas V1 the negative for the calculation of sensitivity and specificity.

Despite the irregularity of correlation-driven organization at the V1-RL border which was identified by the ROC analysis of response timescale, a topographic illustration of the cells within the transition of visual areas demonstrated a pattern of segmentation (Figure 20). Cells within the RL patch that were assigned to V1 based on connectivity, exhibited positive distances from the "criterion" defined by the distribution of response timescales of V1-RL. Therefore, they had higher probability to be associated with V1 compared to RL. The opposite effect was depicted for cells within the V1 patch that were attributed to RL. As a result, response timescale tended to modulate cells at the V1-RL transition zone in such a way that the retinotopic V1-RL border shifted towards RL (Figure 20). In opposition, LM neurons residing within V1 patch were controversially attributed to LM. Concretely, these cells were divided in neurons with either positive or negative distances from "criterion". Consequently, the evaluation of correlation-driven margins was significantly perplexing.

Figure 20

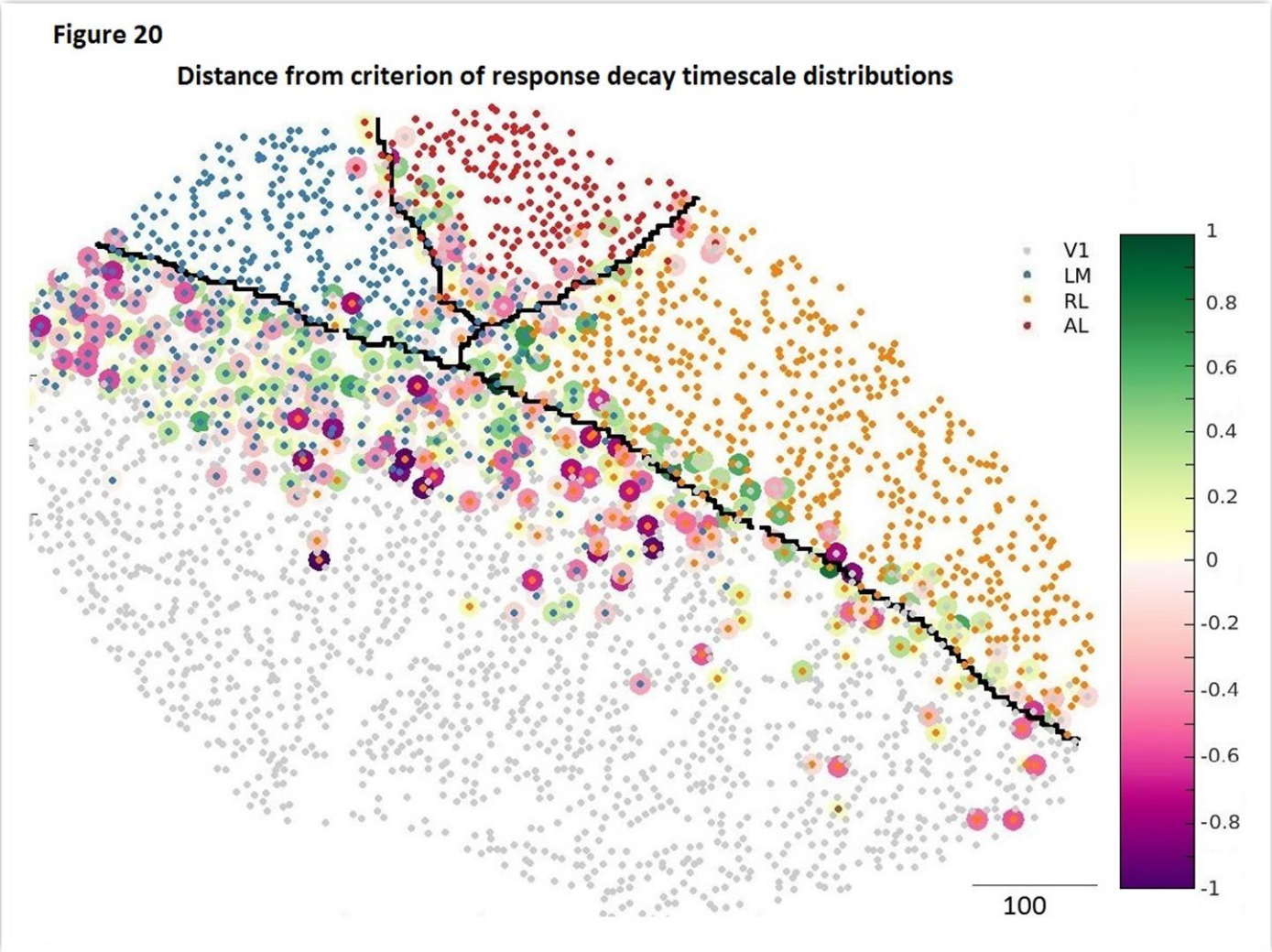

Figure 20. Spatial layout of distance from "criterion" defined by response decay timescale distributions for border cells with opposing labels according to retinotopy and functional connectivity.

V1-RL border organization based on response decay timescale coincide with the connectivity-based expansion of V1 within the RL patch. The other alterations proposed by the connectivity model were inconclusive or even conflicting with the response decay timescale distributions. Bars of 'yellow to green' and 'pink to purple' determine the distance from the intersection point of retinotopic and correlation-driven area distributions. Cells with values from -1 to 0 (purple range dots) represent neurons that did not align with the organization structure of connectivity map, whereas cells within the yellow-green spectrum (i.e. from 0 to 1) concur with the connectivity map. The smaller dots designate the label predicted from NB classifier according to the model generated (V1: grey, RL: orange, LM: blue, AL: red). Black bar describes the size of the scan in pixels (pixel = 2 x 2 µm).

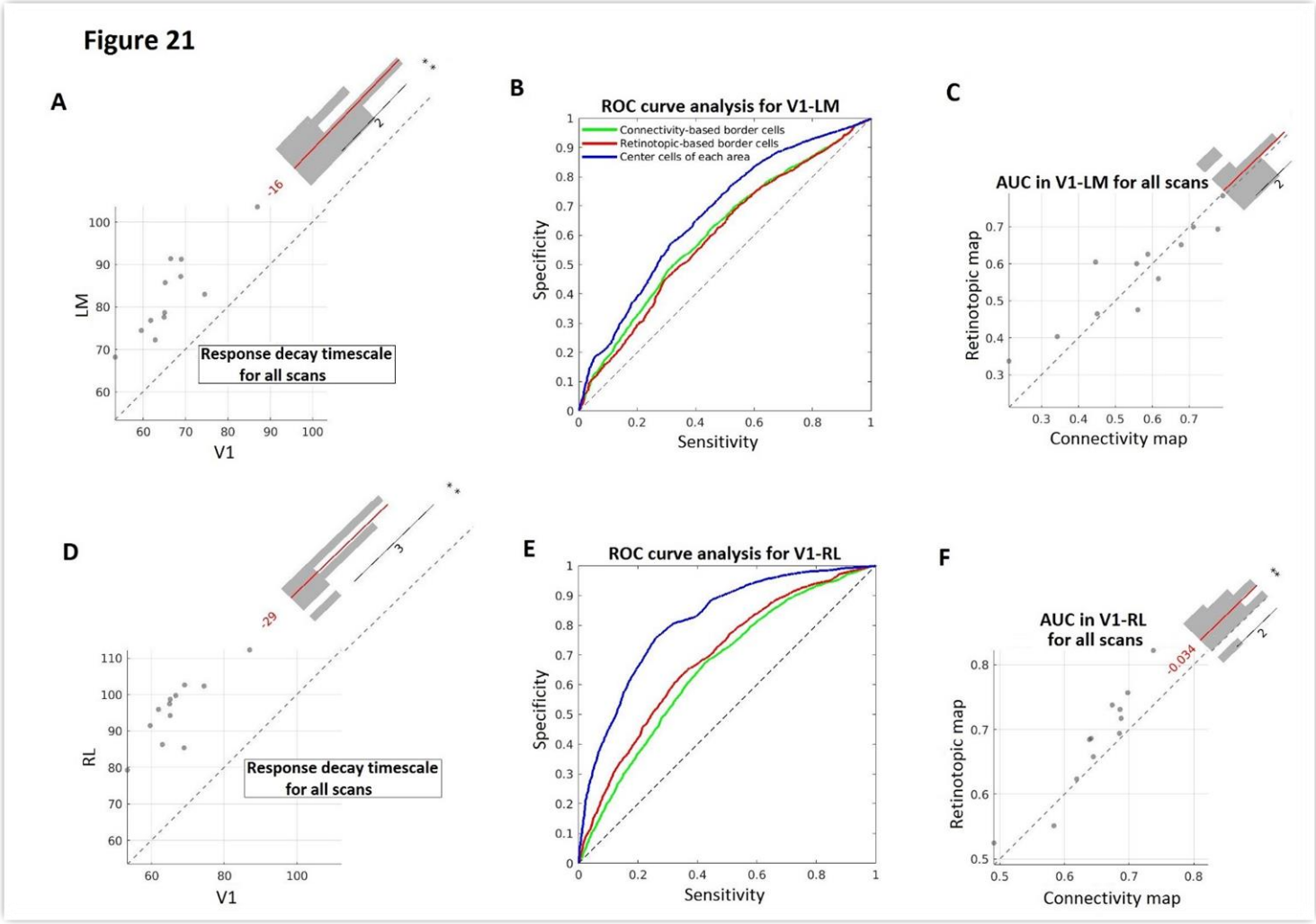

Figure 21. Arrangement of borders based on response decay timescale for all scans.

Only the organization of response timescale at the V1-LM boundary concurs with the connectivity configuration. A, D, Response decay timescale was consistently superior for higher-order areas compared to V1 (t-test: p-value < 0.05). B, E, ROC curves for the comparison of the correlation-driven segmentation of border cells (green line), the retinotopic arrangement of borders (red line) and the center cells of each area (blue line). The response timescale assigns border cells with a slightly improved performance when computed for the correlation-driven labels for V1-LM (B) boundary (green and red line). The opposite outcome was identified for V1-RL transition (E). C, F, AUC analysis over all scans verified the findings for the V1-RL border (t-test: p-value < 0.05). However, this was not the case for V1-LM border (t-test: no statistically significant difference).

In order to establish our findings, the analysis was expanded over all the scans available (Figure 21). V1 was characterized by lower response decay timescales compared to higher-order areas with statistical significance (Figure 21A, 21D). In addition, the ROC curve analysis over all scans could not confirm with confidence our inference for a more adequate organization of V1-LM border based on connectivity compared to the retinotopic topography (Figure 21B). Although the correlation-driven ROC curve seemed to surpass the corresponding curve of retinotopic organization of response timescale, AUC analysis could not reveal a statistically significant difference (Figure 21C). In opposition, V1-RL exhibited adverse results, as the retinotopic segmentation of visual areas assessed more accurately the division of the response decay timescale (Figure 21D, 21E).

Consequently, the same pattern as in previous functional parameters was exhibited (Figure 15, Figure 18). Correlation-driven arrangement of V1-LM border induced distributions of response decay timescale with greater divergence, whereas the opposing effect was demonstrated for V1-RL boundary where the retinotopic organization was superior to connectivity (Figure 21C, 21F).

Chapter 2.2.4 The functional parameters predicted with higher performance the correlation-driven rather than the retinotopic arrangement of borders

Although the functional properties examined in the previous sections could align with the delineation of borders identified with connectivity, in several occasions, these parameters were inconclusive or even conflicting with the correlation-driven labels. In order to further inquire into the validity of correlation-generated map and its differentiation from retinotopic map, the results were evaluated by employing a classification technique relied on the entire scope of functional characteristics examined in previous sections (Chapter 2.2.1, 2.2.2, 2.2.3). The decoder was trained on (i) reliability, (ii) state-dependence and (iii) response decay timescale. These functional parameters were subsequently supplied to a Naïve Bayes classifier with the intention of predicting the class of the testing neurons. In order to generate comparable conditions for the evaluation of the model accuracy, 50% of the cells from each area located at the area's center was treated as the training set and, thus, the classifier's accuracy was computed for the border cells based on the correlation-driven or retinotopic labels. NB had greater

accuracy for the identification of correlation-driven visual areas (29%) compared to retinotopic map (24%). Therefore, neurons with strong connections were defined by similar functional properties and tended to exist in the same visual area. However, the performances of the decoder are significantly low. Further investigations, need to be made in order to identify additional functional parameters that could segment visual cortex.

Chapter 2.3 Connectivity map generated from neural activity of cells in variable layers of brain cortex

Chapter 2.3.1 Consistency of border location for variable depths of brain cortex

When attempting to define the location of boundaries is extremely significant for the validity of the results to determine the situation along every layer. Therefore, data obtained by another mouse, were utilized to evaluate the consistency of correlation-determined borders over varying depths (Figure 22A). The shift of the borders relative to the retinotopic boundaries and the ambiguity of the cell identity nearby the margins of visual areas was evident (Figure 22B). The attention focused on the transition of V1 to LM and RL. The quantification of the border displacement relied on a linear Support Vector Machine (SVM). The coordinates of cells along the border were projected into the line perpendicular to the retinotopic boundary. The decision boundary identified by the linear SVM in the one dimensional space was the proposed location of the borders according to the neural density (see Methods). The findings were beyond dispute invariant across a diverse range of depths for both V1-LM and V1-RL border (Figure 22C, 22D).

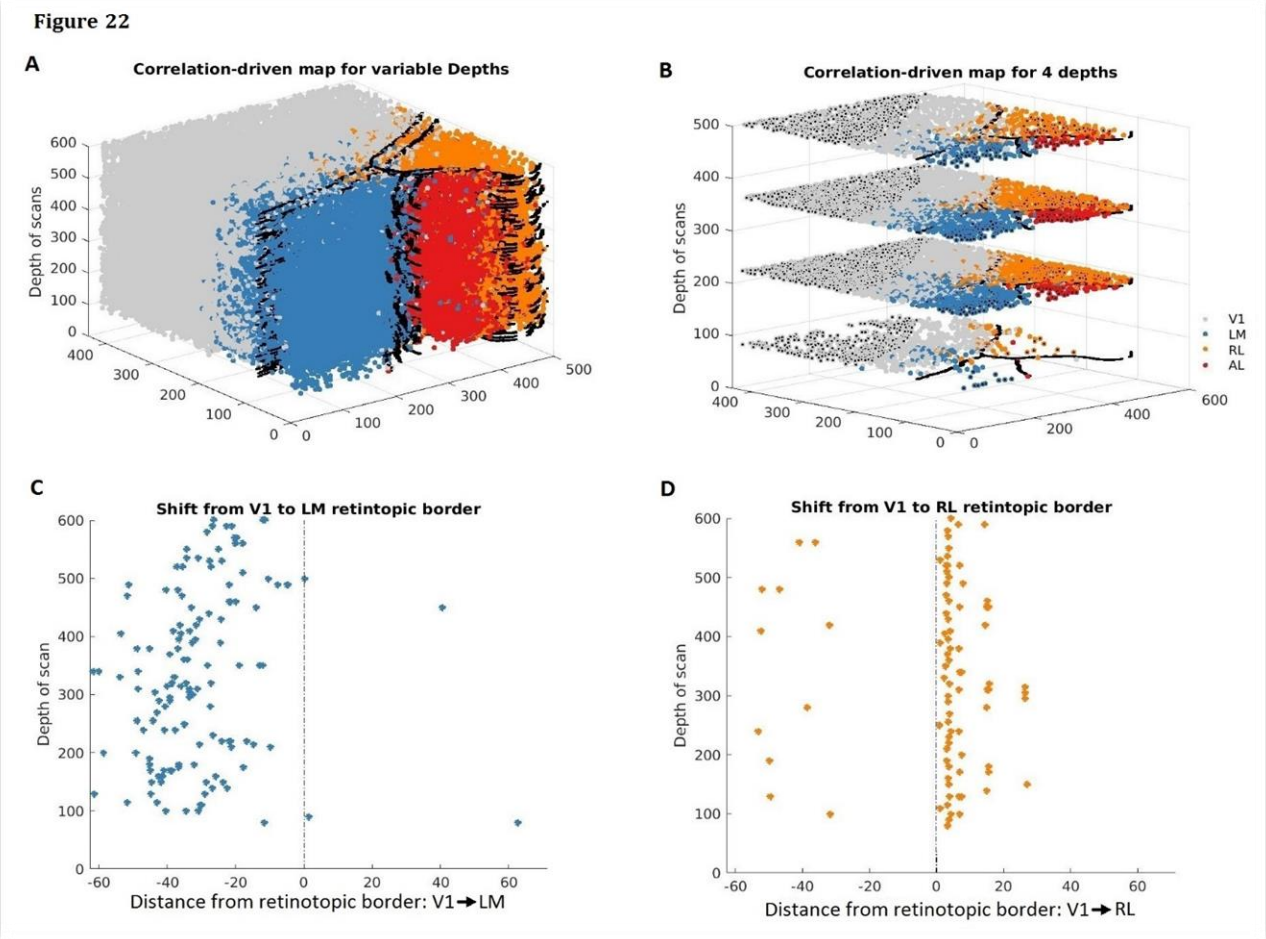

Figure 22. Consistency of border displacement in variable depths.

A, Correlation-driven map for all the depths. Colors of each cell determines the predictions of NB classifier (V1: grey, LM: blue, RL: orange, AL: red). B, Better visualization of cell predictions displayed for 4 example depths. Black dots represent the training samples. C, D, Location of the decision boundary identified by SVM for the data projected into the perpendicular to the retinotopic border line. Shift of V1-LM border towards V1 for variable depths (C) and almost identical to retinotopic border but with a small shift of V1-RL border in the direction of RL (D). Dotted black line designates the retinotopic border.

Chapter 2.3.2 Divergence among the location of borders defined by the neural density and the minimum of neural correlations

To evaluate how correlation conducted across the margins of visual cortex, the same analysis was performed as in Figure 7, but this time for every scan depth. The distance from the border corresponding to the drop of correlation amplitude maintained similar values across the majority of depths (Figure 23A, 23B). Although the lowest point of the inversed U-shaped curve of the mean correlation concurred with the SVM decision boundary (Figure 23C) in reference to the direction of the V1-LM border displacement, the degree of the shift was more extensive compared to SVM positioning (Figure 23C). Since PCA+LDA algorithm assigns neurons nearby the boundaries using 'noise' correlation as the attributing criterion, it was expected that the minimum value of correlations would correspond to the location of neural density transition. However, this was not the case. The location of the border defined by the neural density of the correlation-driven labels and by the position corresponding to the lowest point of 'noise' correlations were in dispute.

Nonetheless, the fact that neighboring areas were characterized by overlapping regions of ambiguous neural identity must not be neglected. In addition, in a previous section (Chapter 2.1.3, Figure 5, 6), 'noise' correlations of higher-order areas were underlined for their superiority over the primary visual cortex. Considering these two observations it is possible to explain the shape of the mean correlation curve (Figure 23). By examining the amplitude of correlation from the center of V1 towards LM, it is possible to discriminate 3 stages of transition within the borders, based on the density of cells from each area that could potentially interpret the disagreement among the two proposed location of boundaries between V1 and LM or RL. Initially, correlations among V1 cells which dominate the first subregion of the border smoothly diminish reaching the minimum while approaching the margin. Next, the pure V1 population is mixed with LM cells which are defined by superior correlations from V1 border cells. As a consequence, mean correlation start to increase and continue to increase as the proportion of LM transcends V1. The same concept applies for V1-RL border (Figure 23B, 23D).

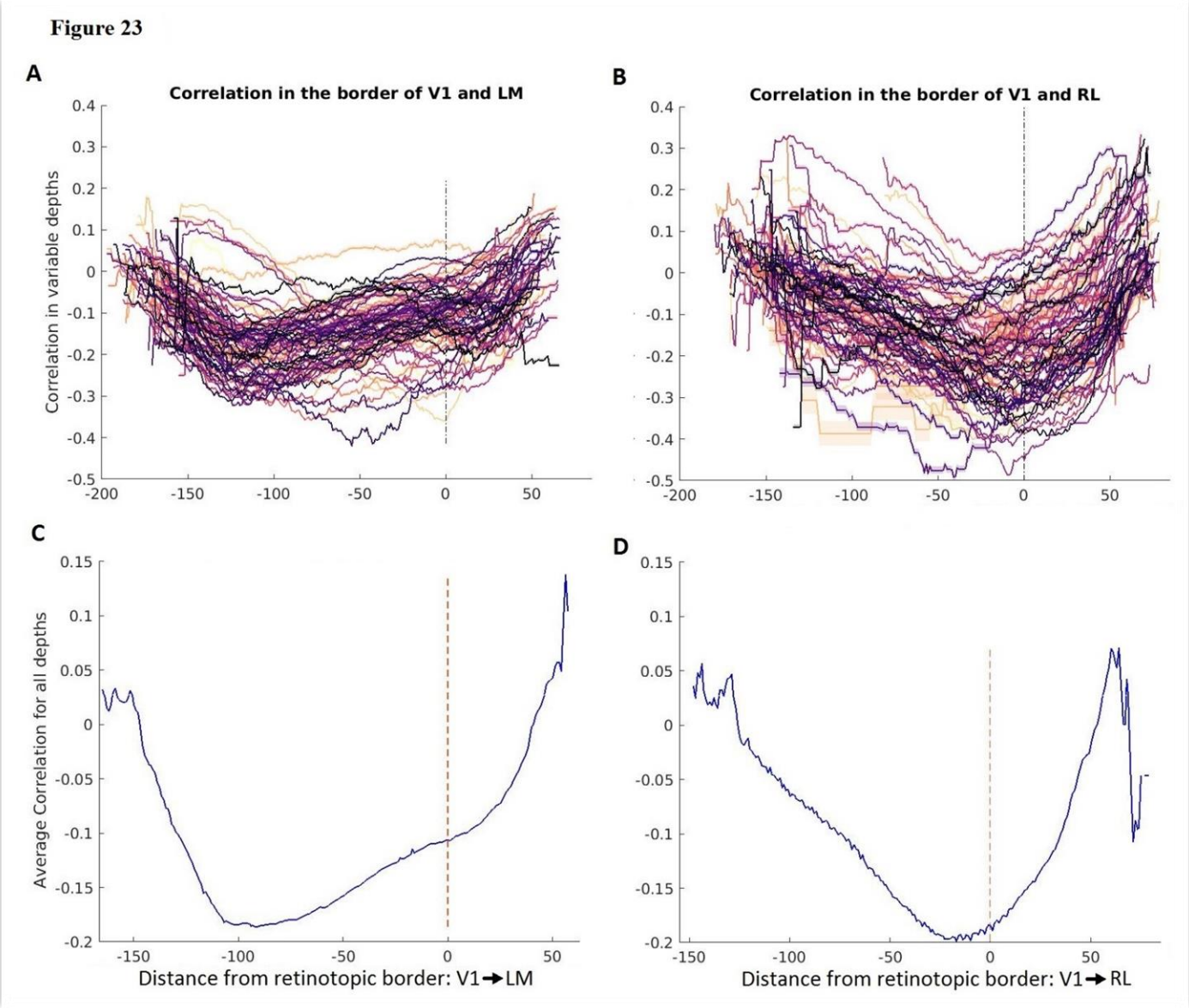

Figure 23. Consistency of correlations decrease in transition zones of V1 and high-order areas boundaries for variable depths.

A, B, Inversed U-shaped curve of correlation identified for variable depths. The lowest point of the correlation amplitude coincides for the majority of depths both for V1-LM (A) and V1-RL (B) border. The vertical line denotes the retinotopic border. The color of each curve reflects the depth of each scan. The spectrum of yellow to purple corresponds to lower to higher values of depth, respectively. C, D, Average correlation across all depths as a function of distance from the relative retinotopic border. Distance measured in pixels (pixel = 2 x 2 µm).

Chapter 2.3.3 t-SNE projects 'noise' data to a space with highly segmented visual areas

The most common method for dimensionality reduction of neural data is principal component analysis (Cunningham and Yu 2014). PCA identifies the ordered set of orthogonal directions that captures the greatest variance in the data. In order to represent the fluctuations around the stimulus-driven responses ('noise'), a 'trial-concatenated PCA' was employed which retained the variability across multiple trials (Yu et al. 2009), (Williams et al. 2018). As a result, this procedure uses an orthogonal transformation to convert an assembly of correlated temporal dimensions into a component which optimally represents the neural correlations of a visual area. The dependence of the orthonormal basis ensures the generation of axis which promote the establishment of a lower dimensional space, where cells of dissimilar fluctuations are mostly separable.

This assumption is, however, motivated by mathematical convenience rather than biological principles. In real biological networks, temporal firing patterns might be correlated in non-orthogonal or non-linear structures that cannot be recovered by PCA. In this perspective, 'noise' data were projected into a lower dimensional space through t-distributed stochastic neighbor embedding (t-SNE). The t-SNE algorithm is a probabilistic approach that maintains neuronal pairwise dissimilarities describing the high-dimensional space to a 2- or 3-D space. Since the purpose was to retain the proximity of cells based on connectivity, the similarity metric used for the probabilistic approach of t-SNE was the correlation coefficients rather than Euclidean distances. The lower dimensional space demonstrated a considerable segmentation of visual areas (Figure 24). Therefore, 'noise' correlations were validated for their capability to distinguish visual areas.

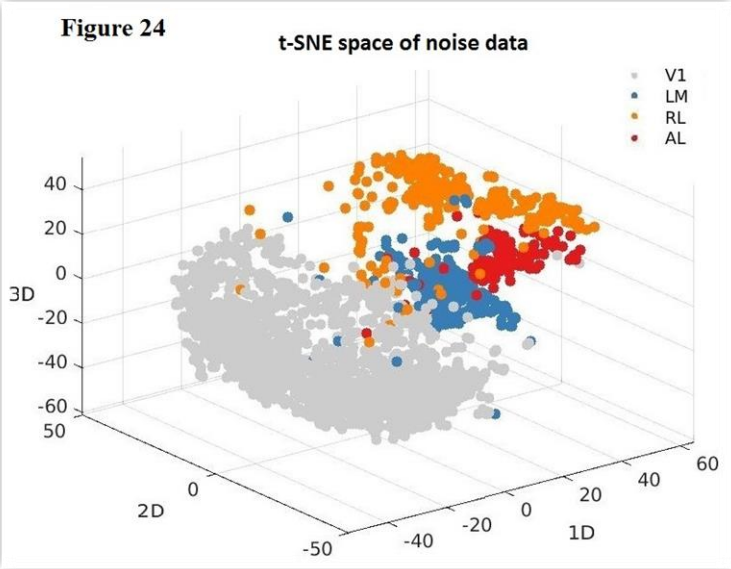

Figure 24. t-SNE space demonstrated considerable segmentations of visual areas

t-SNE projection of 'noise' data (i.e. preprocessing of data in an identical manner as in 'trial-concatenated PCA' algorithm until the application of PCA, step2 in Figure 2B). Only center cells are exhibited. Colors represent the visual area corresponding to the center cells.

Chapter 3. Discussion

As the delineation of areal boundaries is a fundamental procedure for the exploration of visual information encoding, an attempt was made to identify functional mechanisms that distinguish neurons in unique clusters. Understanding how neural networks are organized in order to promote visual perception is an essential step towards interpreting sensory processing. Therefore, we focused on assessing how cortical circuits interact and cooperate to perform complicated computations. In this concept, correlations were used as metric of functional connectivity. Theoretically, neurons would be more associated with cells that share similar neural activity. Therefore, functional connectivity is a potential candidate for identifying distinct structures in the visual cortex corresponding to the visual areas defined by anatomical and retinotopic characteristics.

PCA was the ideal conductor to mediate correlations as it is a dimensionality reduction technique that embodies orthogonal linearity mechanisms. These operations establish a space where uncorrelated structures are substantially separable. Given that intra-area correlation is a dominant characteristic of neural activity (White et al. 2011), (Kumar et al. 2021), principal components would capture the temporal dimensions that are highly correlated due to co-fluctuations of cells within the same visual area.

'Signal' was extracted by averaging data across trials with repeated stimuli. This manipulation is used for disengaging stimulus-driven neural responses from trial-to-trial variability. Functional connectivity maps emerged from 'signal' correlations were inconclusive and could not provide connectivity patterns that would form discrete areas (Figure 3C, 3D). Based on our model, the majority of V1 cells residing close to the boundaries were attributed to higher-order areas (Figure 2A). Therefore, neural responses of V1 border cells are similar to the responses of the cells from higher visual areas. This is possibly due to the resemblance of border cell azimuth with the regions centered within visual areas of higher level of hierarchy (Figure 1A). Retinotopy drastically impacts 'signal' by determining the time points of cell excitability due to the selectivity of neural responses to small parts of visual field.

The classification of border cells portrays a displacement of retinotopic borders towards V1 for the majority of scans and particularly the occupation of V1 regions by LM. The rearrangement of the borders was consistent across the cortical depth (Figure 23). The idea for reconsidering

the accuracy of retinotopic borders has already been proposed when a mismatch in border location was found, indicating that retinotopic transition could not align with architectonic borders (Zhuang et al. 2017). However, the direction of border displacement compared to retinotopic maps, for anatomical and functional connectivity map were opposing (Zhuang et al. 2017). Therefore, the simultaneous assessment of retinotopic, correlation-driven and anatomical borders is deemed necessary in order to fully characterize the border cells.

Moreover, regions close to the border were described by ambiguous neural membership. This is attributed to the mixture of selectivity along the boundaries, which induces a continuum of functional properties rather than a clean separation of regions (Song et al. 2014). The significant variance of retinotopic information and the wide transition of architectonic changes along the borders comes to an agreement with the overlapping visual areas emerged from functional connectivity (Gămănuț et al. 2018), (Zhuang et al. 2017).

Furthermore, the spatial layout of correlations displayed robust connections within the center of each area which progressively diminished approaching the margins of visual area (Figure 5, 7). Although the preferred cell directionality managed to organize structures of pinwheels located at the center of each area, particularly for AL, the computation of the preferable orientation for each neuron revealed substantial variance, especially for border cells (Figure 8, 9). As a consequence, similarity in encoding is highly dependent to the spatial proximity, even for adjacent neurons with opposing labels (Song et al. 2014). It is possible that the equivocal configuration of neural identity within boundaries might be induced by the overlapping afferent projections to the border cells (Juavinett et al. 2016).

Many researchers have argued that the provocation of attention and reward during the trial improves the behavioral performance of the mouse due to the amelioration of signal-to-noise ratio (Cohen and Maunsell 2009). The decrease of 'noise' correlation and the amplification of the firing rate leads to better decoding performance of neural activity (Moore, Khang, and Francis 2020). The opposing effect is mediated when mice watch the movie passively. The establishment of experimental procedures that could describe the mouse attention, learning or reward state, might further improve our understanding for the provenance of 'noise' correlation and possibly enhance the capability of 'signal' correlations to delineate the borders of visual areas.

In order to gain better insight into the architectonic of mouse visual system, functional properties that would comply with visual hierarchy were investigated. The variance explaining

the stimulus-driven responses normalized by the total variance in the primary visual cortex exceeded the mean values of higher-order areas. Hence, the signals of V1 neurons were less contaminated by 'noise'. In agreement with previous research, LM and RL exhibited significantly higher response decay timescales and, therefore, maintained stimulus-evoked activity over longer temporal windows (Siegle et al. 2021). Surprisingly, although all visual areas provided evidence for the state dependence of neural excitability relative to the mouse arousal, only V1 demonstrated higher firing rates for the active state compared to the quiet.

In an attempt to capture the whole functional spectrum of neuronal divergence in the visual cortex, the study oriented towards the identification of multiple functional parameters. The preferred optical flow of each movie, as described by Lucas-Kanade, was one of them (Patel and Upadhyay 2013), (see Methods). However, the distributions of the selective amplitudes of motion vectors for each visual area could not be distinguished. The same issue emerged from signal-to-noise computations (see Methods). By estimating the ratio of variance among the center and periphery of the receptive fields as in Froudarakis et al. 2020, no significant difference between the distributions of V1, LM, and RL could be identified. Therefore, noise generated from receptive field structures have possibly not contributed to the formation of the 'noise' correlation-driven maps. The decoding performance of each cell to predict the identity of the stimulus presented, on the other hand, was not available for all scans. Therefore, it could not be included to the functional parameters that were discriminated between the different visual areas.

In many occasions, the functional parameters exhibited important divergence across visual areas. However, the functional similarities of border cells due to the spatial proximity was a substantial barrier for the identification of distinct divisions. It was evident that the distributions of each area demonstrated notable overlap, probably mirroring the ambiguity exhibited in the borders of the functional connectivity map. Therefore, likely due to the similar afferent projections of adjacent cells, the sharp delineation of definite boundaries might be infeasible and impractical.

Finally, when studying functional connectivity and, especially, when attempting to establish the boundaries of visual cortex induced by neural correlations, it vital not to discount the importance of feedback connections. It is generally accepted that feedback inputs regulate visual processing by modulating the brain state (Briggs 2020). Reciprocal connections and bidirectional interactions across the visual areas facilitate the encoding of visual information

(Liang et al. 2017). Therefore, the ambiguity of neural identity within borders might be elicited due to the feedback interactions. Based on this conviction, there is a great possibility that cells located at the patch of the primary visual cortex were falsely assigned to higher-order areas based on correlation analysis. Concretely, both LM and RL, as defined by functional connectivity, consisted of neurons which penetrated V1 and induced important vagueness at the border.

However, the V1-LM border organization, according to the functional parameters, displayed neurons with greater probabilities to be assigned to the correlation-driven area compared to the retinotopic, especially for reliability. In other words, neurons attributed to LM based on connectivity, could not be falsely identified, since there was an agreement with the topographic layout originated by the functional properties. Nonetheless, the merger of these findings with anatomical ground truth data will eliminate every hesitation.

On the other hand, RL cells consistently concurred with the retinotopic arrangement of the margins. In addition, RL cells within the V1 patch were residing far from the border, with a small likelihood of being associated with RL. Therefore, neurons located at the V1 patch might not be correctly predicted to RL based on connectivity. In fact, these cells might be assigned to RL due to feedback inputs of RL to V1, which enhanced the correlation of neural activity. Therefore, correlation-driven organization of V1-RL border was in dispute with the probabilities emerged from functional parameters.

Chapter 4. Conclusion and recommendations for future research

The elaborate description of the visual system organization is critical for understanding the encoding of visual information in mouse brain and assessing the emergence of visual perception and behavior from cortical areas processing. It is supported that neural connectivity represented in a lower dimensional space of extensive separation among the uncorrelated regional structures, could enrich the anatomical and retinotopic pipeline available for the segmentation of visual cortex. The simultaneous investigation of retinotopic, anatomical and correlation-driven boundaries would guide future experiments targeting the exploration of global topography of visual cortical areas. However, even if functional connectivity map is not representing the actual borders, it is extremely interesting that V1 and higher order areas significantly interact with reciprocal connections.

The resulting connectivity map was generated by 'noise' correlations elicited during the passive presentation of movies. Considering that 'noise' correlations mirror the alternating network states, future experiments should be conducted within conditions which will evoke the awakening of the mouse. By embedding behavioral tasks and rewards during the trial operation, animal states, such as attention, which influence neural co-fluctuations, might facilitate the modulation of correlations.

Finally, although the functional properties that were examined could lay the foundation for confidently delineating the boundaries of visual areas, further research needs to be made for identifying neural parameters with superior separation capacity along the visual hierarchy.

Chapter 5. Methods

Chapter 5.1 Animals and imaging

A total number of 5 adult mice expressing GCaMP6s in excitatory neurons were used. Animals were anesthetized with isoflurane (2%) and a craniotomy was made over the right visual cortex as described in (Froudarakis et al. 2014). The animals were head-fixed on top of a cylindrical treadmill and calcium imaging was performed using Chameleon Ti-Sapphire laser tuned to 920 nm. Calcium traces were recorded using a two-photon resonant microscope with a field of view 1200 x 1200 μm for 12 distinct sessions across 4 mice. For one of the five mice, data were recorder from depths of 100–600 μm below the cortical surface. The field of view for this mice was 500 x 500 μm. Imaging was performed at approximately 5-30Hz for all scans.

Chapter 5.2 Experiment structure and visual stimuli

Mice passively watched several movies during each session. The presentation of the movies was randomly structured. Usually, each session consisted of 6 unique 10s clips presented over 20 times each, with grey screen intervals within the movie presentation and at the end of the session. Movie clips included parts of cinema movies, such as “Mad Max” or “Matrix-Reloaded” or “Matrix-Revolutions”, and objects.

Chapter 5.3 Retinotopic map

For the identification of visual areas, upward and rightward drifting white bars of constant speed and width, on black background, were used as stimuli. In addition, within the bars, drifting gratings with opposite direction to the movement of the bar were added. 2D phase maps constructed for the two directions were used for the delineation of visual cortex, as previously described (Q and A 2007), (Garrett et al. 2014).

Chapter 5.4 Dimensionality reduction and Classification

Before data were embedded into the dimensionality reduction model, several manipulations were performed in order to extract ‘signal’ and ‘noise’ data. For the isolation of stimulus-driven responses, an averaging across trials with identical stimuli was applied in order to disengage trial-to-trial variability from ‘signal’. On the other hand, ‘noise’ was computed by normalizing

the data (z-score) from the zero mean of each neuron calculated for all trials with identical stimuli. In the same direction, spontaneous data obtained from periods of time when a grey screen was presented, were normalized from the cell zero mean activity, calculated for periods of no stimulus. The outcome of the manipulations described above was concatenated in both situations of 'signal' and 'noise', as reported in 'trial-averaged PCA' and 'trial-concatenate PCA' algorithms, respectively (Williams et al. 2018).

Unlike PCA, LDA is a supervised dimensionality reduction method. Therefore, in order to avoid over-fitting biases LDA was applied for a subset of neurons. From each area, half of the neurons were selected as the training set. However, the selection was not random. At first, the distance of each cell from the retinotopic border was measured as the length of the smallest line connecting the cell and the border. Secondarily, a threshold was placed at the 50^{th} percentile of the distance distribution of each area and, then, defined the center cells as training set and the border cells as the testing samples. In this manner, it was possible to make predictions for the cell identities in the border, by minimizing the retinotopic information. In addition, center cells with overlapping horizontal retinotopy to the border cells were excluded from the training set.

A Naïve Bayes classifier was used for predicting the label of border cells, trained on the LDA features of center cells. Because of the inequality describing the number of neurons within each area, the prior probabilities used were uniform for all visual areas. For the convenience of our computations and the better visualization of the connectivity map originated by the NB predictions, cells that were assigned to a visual area and had distance from the class centroid which exceeded 3 standard deviations, were attributed to the cluster with the next higher posterior probability.

Chapter 5.5 Correlation analysis

For the estimation of connectivity parameters of cells adjacent to the boundaries, the interest focused on regions of transition of the primary visual cortex to higher-order areas. All the computations for the neural correlations were applied to the space generated by the dimensionality reductions technique (PCA+LDA). At first, the correlation amplitude was examined along the margins of V1. Rectangles with dimensions 400 x 180 μm were used for the V1-LM boundary and 500 x 230 μm for the RL-V1. The slope of the longer side of the rectangle should be perpendicular to the border, as correlations would be averaged across this

dimension. The rest of the parameters for the selection of the region were insignificant as long as the district included cells from the center of each area.

Next, the correlations of each neural pair were computed within the rectangle and a 2D matrix was constructed with rows equal to the number of neural pairs and columns representing the distance from the border for the two cells defining the row. Its row was filled with the value of pairwise correlation from the column corresponding to the location of the first cell relative to the border, through the column corresponding to the position of the second neuron in reference to its distance from the boundary. The inversed U-shaped curve of correlation amplitude along the border was induced by the averaging of the correlation matrix across the dimension of the rectangle perpendicular to the border. The null-hypothesis was induced by the randomization of the rows in the correlation matrix.

In the same framework, the directionality of each cell was computed within the next steps: 1. Calculation of pairwise correlations for neurons with distance lower than 100 μm, 2. Measurement of the angle describing the connection of each neuron pair. This angle was determined by the line passing over the location of the neural pair and a horizontal line crossing the cell of reference, 3. The power of correlation and the angle computed were translated into a Cartesian space and interpreted as the amplitude and the angle of a vector. The average of the real and imaginary part of the population of vectors defining the connections of each cell induced the preferential neural directionality.

Chapter 5.6 Identification of border location for each scan depth

A linear regression model fitted the border of V1-LM and V1-RL border in order to discover the coefficients and intercept of the line which minimizes the residual sum of squares between the x and y coordinates of the retinotopic border and the prediction of the linear approximation. This step was necessary due to the curvature designating boundaries. Next, the coordinates of every border cell assigned to the visual area of interest was projected into the perpendicular to the border line. The location of the decision boundary identified by the SVM into the 1D space based on the correlation-driven labels defined the position of the connectivity-derived boundary relative to the retinotopic.

Chapter 5.7 Association of functional parameters organization with the connectivity map

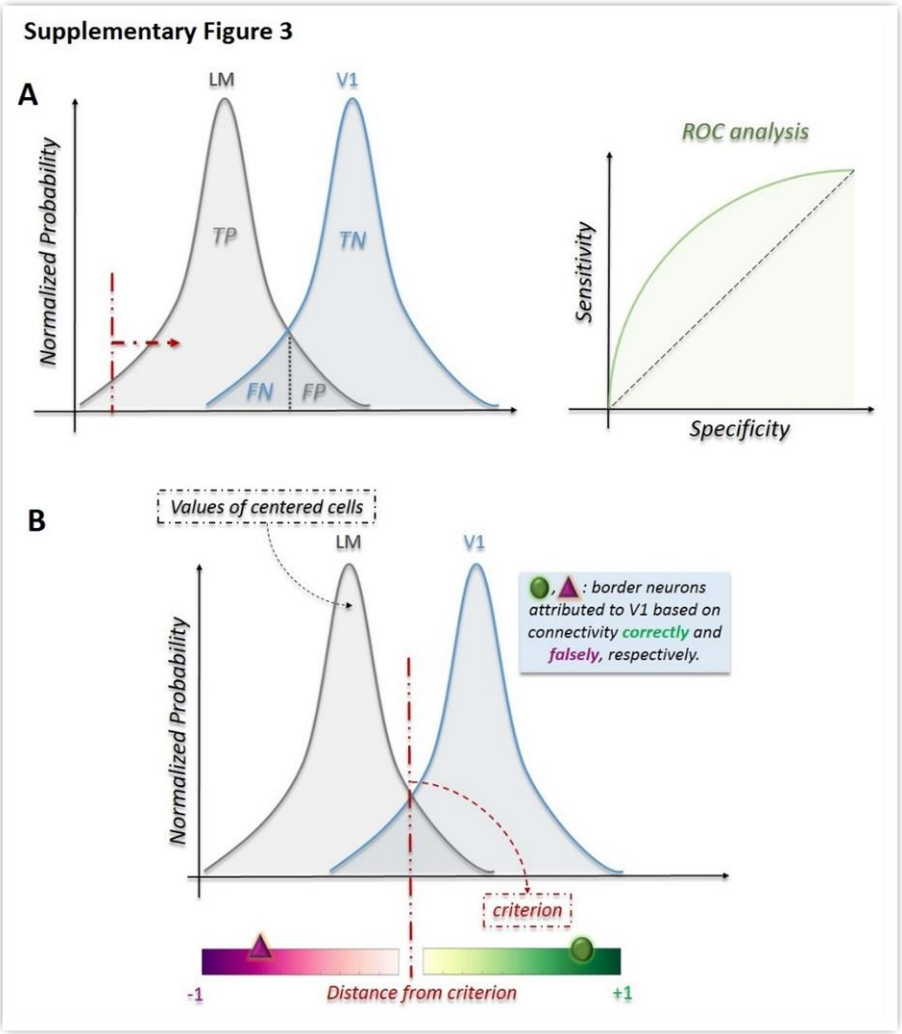

ROC analysis was used as the diagnostic tool of discrimination of neighboring areas. Computations were applied for the distribution of the functional parameter examined. Data were tested for (i) the correlation-driven organization of border cells, (ii) the retinotopic arrangement of boundaries and (iii) the center cells of each area, as the discrimination threshold varied (Supplementary figure 3A, red dotted line). As the threshold was moving, sensitivity reduced due to the False Negative (FN) cells (sensitivity = TP / TP+FN, where TP abbreviates True Positive) and specificity amplified due to the False Positive (FP) cells (specificity = TN / TN+FP, where TN abbreviates True Negative). TP cells were designated by the distribution located at the left. For the illustration of Supplementary figure 3A, LM described the positive class.

For the spatial layout of the functional parameter organization, the "criterion" was calculated, as the point of the intersection for the distributions of the center cells (Supplementary figure 3A, red dotted line). Cells that had opposing labels according to retinotopy and connectivity were investigated in order to examine the area with the higher probability to be assigned based on the functional parameter. For example, a neuron that was attributed to V1 in reference to connectivity, would be correctly labelled if its normalized distance from the criterion was positive (Supplementary figure 3B, green circle), In contrast negative values imply greater possibility to coincide with the retinotopic organization of border (Supplementary figure 3B, purple triangle).

Chapter 5.7 t-SNE applied to functional properties space or 'noise' data

Neuronal pairwise dissimilarities used for the identification of the t-SNE space were measured either by the Euclidean distance of the functional properties space or the pairwise neural correlations for the 'noise' data. The centroids of each visual area within the t-SNE space were calculated including only center cells. By comparing the distance of each border cell that had opposing label according to retinotopy and connectivity, it was possible to define the association of the visual cortex arrangement identified in a non-linear reduced space with the retinotopic or connectivity organization.

Chapter 5.8 Functional parameters computations

Chapter 5.8.1 Reliability

The reliability was computed as the variance of the averaged neural activity across trials with identical stimulus presentation divided by the variance of the responses for all the trials with the same stimulus.

$$\boldsymbol{Reliability} = \frac{\frac{\sum(\boldsymbol{x_i} - \bar{\boldsymbol{x}})^2}{\boldsymbol{n-1}}}{\frac{\sum(\boldsymbol{y_j} - \bar{\boldsymbol{y}})^2}{\boldsymbol{k-1}}}$$

Where $\boldsymbol{x_i}$, for $\boldsymbol{i = 1{:}\,n}$, are the values of the averaged responses of the neuron across the trials with the same stimulus with time length equal to $\boldsymbol{n}$. Additionally, $\boldsymbol{y_j}$ for $\boldsymbol{j = 1{:}\,k}$ is the activity of a neuron for all the trials of total duration $\boldsymbol{k}$.

Chapter 5.8.2 State Dependence

The arousal of mice were calculated by measuring the velocity of the treadmill. Next, a threshold was placed at the 85th percentile of the velocity and divided our data into active and quiet state activity. Therefore, state dependence for each cell was computes as follows,

$$\boldsymbol{State\ Dependence} = \frac{\boldsymbol{FR_{active}} - \boldsymbol{FR_{quiet}}}{\boldsymbol{FR_{active}} + \boldsymbol{FR_{quiet}}}$$

where $\boldsymbol{FR_{active}}$ is the averaged firing rate for the time period that the mouse had velocity lower than the threshold. The same calculation applied for $\boldsymbol{FR_{quiet}}$.

Chapter 5.8.3 Response decay timescale

The neural activity was averaged across trials with the same stimulus and the autocorrelation of each signal was computed. Data were normalized from 0 to 1 and an exponential decay function was fitted with its starting point at [0,1]. The exponential decay constant for each curve defined the response timescale of each neuron for each movie. The ultimate response decay timescale for each cell was defined by the mean decay constant across all movie presentations.

Chapter 5.8.4 Decoding performance

The decoding performance of each cell was computed as in Froudarakis et al. 2020. A one-versus-all logistic regression was used for predicting the movie identity based on the neural activity. The performance of the decoder was tested on 10% of the data that were held out during training and a 10 fold cross-validation was used.

The same procedure was employed for predicting the identity of movies with moving objects whose attributes were transforming during each trials. The generalization decoding performance referred to space parameters of the moving object, including changes in translation (x and y), pose (tilt and rotation), scale and light (3 light sources) (Froudarakis et al. 2020). For the generalization performance across object parameters, the decoder was trained on 75% and the accuracy of the classifier was cross-validated in a 4 fold manner.

Chapter 5.8.5 Signal-to-noise ratio of receptive field

The receptive field locations and sizes were mapped using black and white squares that covered 10 degrees of the visual field as in Froudarakis et al. 2020. Stimulus was presented across the whole monitor in random order for 150-200 ms. The ratio of variance in the 2D map within 3 standard deviations from the center of the receptive field to the variance outside this limit measured the SNR.

Chapter 5.8.6 Motion amplitude preference

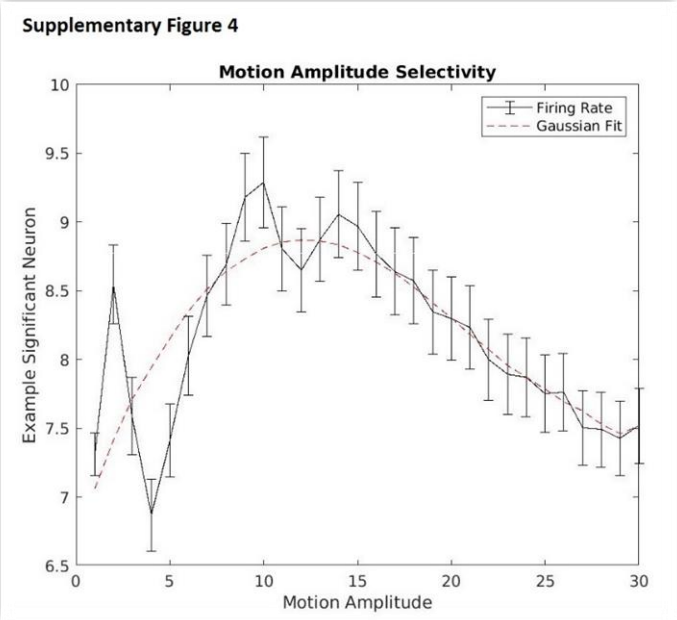

At first, the amplitude of the motion vector for each movie frame was calculated based on Lucas-Kanade (Patel and Upadhyay 2013) and averaged for the center pixels of each frame. Next, the mean firing ratewas computed for each of the 30 bins of motion amplitude (Supplementary Figure 4, black line). A 2nd order Gaussian function was fitted in the mean firing rates of each cell along the 30 bins (Supplementary Figure 4, red line). The preferred motion amplitude for each cell was the value corresponding to the maximum of the fitted curve. Only cells with statistically significant differences of the firing rates within the highest and lowest neural activity bin of motion amplitude were included into the analysis.

Chapter 6. References

Andermann, Mark L., Aaron M. Kerlin, Demetris K. Roumis, Lindsey L. Glickfeld, and R. Clay Reid. 2011. “Functional Specialization of Mouse Higher Visual Cortical Areas.” *Neuron* 72(6):1025–39.

Averbeck, Bruno B., Peter E. Latham, and Alexandre Pouget. 2006. “Neural Correlations, Population Coding and Computation.” *Nature Reviews Neuroscience 2006 7:5* 7(5):358–66.

Briggs, Farran. 2020. “Role of Feedback Connections in Central Visual Processing.” *Annual Review of Vision Science* 6:313–34.

Cohen, Marlene R., and Adam Kohn. 2011. “Measuring and Interpreting Neuronal Correlations.” *Nature Neuroscience 2011 14:7* 14(7):811–19.

Cohen, Marlene R., and John H. R. Maunsell. 2009. “Attention Improves Performance Primarily by Reducing Interneuronal Correlations.” *Nature Neuroscience 2009 12:12* 12(12):1594–1600.

Cohen, Marlene R., and William T. Newsome. 2008. “Context-Dependent Changes in Functional Circuitry in Visual Area MT.” *Neuron* 60(1):162–73.

Cunningham, John P., and Byron M. Yu. 2014. “Dimensionality Reduction for Large-Scale Neural Recordings.” *Nature Neuroscience 2014 17:11* 17(11):1500–1509.

Doiron, Brent, Ashok Litwin-Kumar, Robert Rosenbaum, Gabriel K. Ocker, and Krešimir JosiC. 2016. “The Mechanics of State Dependent Neural Correlations.” *Nature Neuroscience* 19(3):383.

Ecker, Alexander S., Philipp Berens, R. James Cotton, Manivannan Subramaniyan, George H. Denfield, Cathryn R. Cadwell, Stelios M. Smirnakis, Matthias Bethge, and Andreas S. Tolias. 2014. “State Dependence of Noise Correlations in Macaque Primary Visual Cortex.” *Neuron* 82(1):235–48.

Ecker, Alexander S., Philipp Berens, Georgios A. Keliris, Matthias Bethge, Nikos K. Logothetis, and Andreas S. Tolias. 2010. “Decorrelated Neuronal Firing in Cortical Microcircuits.” *Science (New York, N.Y.)* 327(5965):584–87.

Esfahany, Kathleen, Isabel Siergiej, Yuan Zhao, and Il Memming Park. 2018. “Organization of Neural Population Code in Mouse Visual System.” *ENeuro* 5(4).

Fahey, Paul G., Taliah Muhammad, Cameron Smith, Emmanouil Froudarakis, Erick Cobos,

Jiakun Fu, Edgar Y. Walker, Dimitri Yatsenko, Fabian H. Sinz, Jacob Reimer, and Andreas S. Tolias. 2019. “A Global Map of Orientation Tuning in Mouse Visual Cortex.” *BioRxiv*.

Field, David J. 1987. “Relations between the Statistics of Natural Images and the Response Properties of Cortical Cells.” *JOSA A, Vol. 4, Issue 12, Pp. 2379-2394* 4(12):2379–94.

Froudarakis, Emmanouil, Philipp Berens, Alexander S. Ecker, R. James Cotton, Fabian H. Sinz, Dimitri Yatsenko, Peter Saggau, Matthias Bethge, and Andreas S. Tolias. 2014. “Population Code in Mouse V1 Facilitates Readout of Natural Scenes through Increased Sparseness.” *Nature Neuroscience 2014 17:6* 17(6):851–57.

Froudarakis, Emmanouil, Uri Cohen, Maria Diamantaki, Edgar Y. Walker, Jacob Reimer, Philipp Berens, Haim Sompolinsky, and Andreas S. Tolias. 2020. “Object Manifold Geometry across the Mouse Cortical Visual Hierarchy.” *BioRxiv* 2020.08.20.258798.

Gămănuţ, Răzvan, Henry Kennedy, Zoltán Toroczkai, Mária Ercsey-Ravasz, David C. Van Essen, Kenneth Knoblauch, and Andreas Burkhalter. 2018. “The Mouse Cortical Connectome, Characterized by an Ultra-Dense Cortical Graph, Maintains Specificity by Distinct Connectivity Profiles.” *Neuron* 97(3):698-715.e10.

Ganesh Kumar, Mari, I. D. 1☯, Ming Hu, I. D. 2☯, Aadhirai Ramanujan Id, Mriganka Sur, and Hema A. Murthy Id. 2021. “Functional Parcellation of Mouse Visual Cortex Using Statistical Techniques Reveals Response-Dependent Clustering of Cortical Processing Areas.”

Garrett, Marina E., Ian Nauhaus, James H. Marshel, and Edward M. Callaway. 2014. “Topography and Areal Organization of Mouse Visual Cortex.” *Journal of Neuroscience* 34(37):12587–600.

Gilbert, Charles D., and Wu Li. 2013. “Top-down Influences on Visual Processing.” *Nature Reviews Neuroscience 2013 14:5* 14(5):350–63.

Glickfeld, Lindsey L., Mark L. Andermann, Vincent Bonin, and R. Clay Reid. 2013. “Cortico-Cortical Projections in Mouse Visual Cortex Are Functionally Target Specific.” *Nature Neuroscience* 16(2):219–26.

Gu, Yong, Sheng Liu, Christopher R. Fetsch, Yun Yang, Sam Fok, Adhira Sunkara, Gregory C. DeAngelis, and Dora E. Angelaki. 2011. “Perceptual Learning Reduces Interneuronal Correlations in Macaque Visual Cortex.” *Neuron* 71(4):750.

Gur, Moshe, and D. Max Snodderly. 2006. “High Response Reliability of Neurons in Primary Visual Cortex (V1) of Alert, Trained Monkeys.” *Cerebral Cortex* 16(6):888–95.

Harris, Kenneth D., and Thomas D. Mrsic-Flogel. 2013. “Cortical Connectivity and Sensory Coding.”

Heggelund, P., and K. Albus. 1978. “Response Variability and Orientation Discrimination of Single Cells in Striate Cortex of Cat.” *Experimental Brain Research* 32(2):197–211.

JH, Marshel, Garrett ME, Nauhaus I, and Callaway EM. 2011. “Functional Specialization of Seven Mouse Visual Cortical Areas.” *Neuron* 72(6):1040–54.

Juavinett, Ashley L., Euiseok J. Kim, Hannah C. Collins, and Edward M. Callaway. 2020. “A Systematic Topographical Relationship between Mouse Lateral Posterior Thalamic Neurons and Their Visual Cortical Projection Targets.” *The Journal of Comparative Neurology* 528(1):95.

Juavinett, Ashley L., Ian Nauhaus, Marina E. Garrett, Jun Zhuang, and Edward M. Callaway. 2016. “Automated Identification of Mouse Visual Areas with Intrinsic Signal Imaging.” *Nature Protocols 2016 12:1* 12(1):32–43.

Kalatsky, Valery A., and Michael P. Stryker. 2003. “New Paradigm for Optical Imaging: Temporally Encoded Maps of Intrinsic Signal.” *Neuron* 38(4):529–45.

Kayser, Christoph, Konrad P. Körding, and Peter König. 2004. “Processing of Complex Stimuli and Natural Scenes in the Visual Cortex.” *Current Opinion in Neurobiology* 14(4):468–73.

Ko, Ho, Sonja B. Hofer, Bruno Pichler, Katherine A. Buchanan, P. Jesper Sjöström, and Thomas D. Mrsic-Flogel. 2011. “Functional Specificity of Local Synaptic Connections in Neocortical Networks.” *Nature 2011 473:7345* 473(7345):87–91.

Kumar, Mari Ganesh, Ming Hu, Aadhirai Ramanujan, Mriganka Sur, and Hema A. Murthy. 2021. “Functional Parcellation of Mouse Visual Cortex Using Statistical Techniques Reveals Response-Dependent Clustering of Cortical Processing Areas.” *PLOS Computational Biology* 17(2):e1008548.

Laramée, Marie Eve, and Denis Boire. 2015. “Visual Cortical Areas of the Mouse: Comparison of Parcellation and Network Structure with Primates.” *Frontiers in Neural Circuits* 8(JAN):149.

Lennie, Peter. 1998. “Single Units and Visual Cortical Organization.” *Perception* 27(8):889–935.

Liang, Hualou, Xiajing Gong, Minggui Chen, Yin Yan, Wu Li, and Charles D. Gilbert. 2017. “Interactions between Feedback and Lateral Connections in the Primary Visual Cortex.” *Proceedings of the National Academy of Sciences of the United States of America*

114(32):8637–42.

Marshel, James H., Marina E. Garrett, Ian Nauhaus, and Edward M. Callaway. 2011. "Functional Specialization of Seven Mouse Visual Cortical Areas." *Neuron* 72(6):1040–54.

Merrikhi, Yaser, Kelsey Clark, and Behrad Noudoost. 2018. "Concurrent Influence of Top-down and Bottom-up Inputs on Correlated Activity of Macaque Extrastriate Neurons." *Nature Communications 2018 9:1* 9(1):1–12.

Moore, Brittany, Sheng Khang, and Joseph Thachil Francis. 2020. "Noise-Correlation Is Modulated by Reward Expectation in the Primary Motor Cortex Bilaterally During Manual and Observational Tasks in Primates." *Frontiers in Behavioral Neuroscience* 14:192.

Nirenberg, Sheila, and Peter E. Latham. 2003. "Decoding Neuronal Spike Trains: How Important Are Correlations?" *Proceedings of the National Academy of Sciences* 100(12):7348–53.

Olavarria, Jaime, and Vicente M. Montero. 1989. "Organization of Visual Cortex in the Mouse Revealed by Correlating Callosal and Striate-Extrastriate Connections." *Visual Neuroscience* 3(1):59–69.

Patel, Dhara, and Saurabh Upadhyay. 2013. "Optical Flow Measurement Using Lucas Kanade Method." *International Journal of Computer Applications* 61(10):975–8887.

Perin, Rodrigo, Thomas K. Berger, and Henry Markram. 2011. "A Synaptic Organizing Principle for Cortical Neuronal Groups." *Proceedings of the National Academy of Sciences of the United States of America* 108(13):5419–24.

Piasini, Eugenio, Liviu Soltuzu, Paolo Muratore, Riccardo Caramellino, Kasper Vinken, Hans Op de Beeck, Vijay Balasubramanian, and Davide Zoccolan. 2021. "Temporal Stability of Stimulus Representation Increases along Rodent Visual Cortical Hierarchies." *Nature Communications 2021 12:1* 12(1):1–19.

Q, Wang, and Burkhalter A. 2007. "Area Map of Mouse Visual Cortex." *The Journal of Comparative Neurology* 502(3):339–57.

Schuett, Sven, Tobias Bonhoeffer, and Mark Hübener. 2002. "Mapping Retinotopic Structure in Mouse Visual Cortex with Optical Imaging." *Journal of Neuroscience* 22(15):6549–59.

Sherman, S. Murray, and R. W. Guillery. 1998. "On the Actions That One Nerve Cell Can Have on Another: Distinguishing 'Drivers' from 'Modulators.'" *Proceedings of the National*

Academy of Sciences 95(12):7121–26.

Siegle, Joshua H., Xiaoxuan Jia, Séverine Durand, Sam Gale, Corbett Bennett, Nile Graddis, Greggory Heller, Tamina K. Ramirez, Hannah Choi, Jennifer A. Luviano, Peter A. Groblewski, Ruweida Ahmed, Anton Arkhipov, Amy Bernard, Yazan N. Billeh, Dillan Brown, Michael A. Buice, Nicolas Cain, Shiella Caldejon, Linzy Casal, Andrew Cho, Maggie Chvilicek, Timothy C. Cox, Kael Dai, Daniel J. Denman, Saskia E. J. de Vries, Roald Dietzman, Luke Esposito, Colin Farrell, David Feng, John Galbraith, Marina Garrett, Emily C. Gelfand, Nicole Hancock, Julie A. Harris, Robert Howard, Brian Hu, Ross Hytnen, Ramakrishnan Iyer, Erika Jessett, Katelyn Johnson, India Kato, Justin Kiggins, Sophie Lambert, Jerome Lecoq, Peter Ledochowitsch, Jung Hoon Lee, Arielle Leon, Yang Li, Elizabeth Liang, Fuhui Long, Kyla Mace, Jose Melchior, Daniel Millman, Tyler Mollenkopf, Chelsea Nayan, Lydia Ng, Kiet Ngo, Thuyahn Nguyen, Philip R. Nicovich, Kat North, Gabriel Koch Ocker, Doug Ollerenshaw, Michael Oliver, Marius Pachitariu, Jed Perkins, Melissa Reding, David Reid, Miranda Robertson, Kara Ronellenfitch, Sam Seid, Cliff Slaughterbeck, Michelle Stoecklin, David Sullivan, Ben Sutton, Jackie Swapp, Carol Thompson, Kristen Turner, Wayne Wakeman, Jennifer D. Whitesell, Derric Williams, Ali Williford, Rob Young, Hongkui Zeng, Sarah Naylor, John W. Phillips, R. Clay Reid, Stefan Mihalas, Shawn R. Olsen, and Christof Koch. 2021. “Survey of Spiking in the Mouse Visual System Reveals Functional Hierarchy.” *Nature* 592(7852):86–92.

Song, H. Francis, Henry Kennedy, and Xiao Jing Wang. 2014. “Spatial Embedding of Structural Similarity in the Cerebral Cortex.” *Proceedings of the National Academy of Sciences of the United States of America* 111(46):16580–85.

Vinck, Martin, Renata Batista-Brito, Ulf Knoblich, and Jessica A. Cardin. 2015. “Arousal and Locomotion Make Distinct Contributions to Cortical Activity Patterns and Visual Encoding.” *Neuron* 86(3):740–54.

Vinje, William E., and Jack L. Gallant. 2000. “Sparse Coding and Decorrelation in Primary Visual Cortex during Natural Vision.” *Science (New York, N.Y.)* 287(5456):1273–76.

White, Brian R., Adam Q. Bauer, Abraham Z. Snyder, Bradley L. Schlaggar, Jin Moo Lee, and Joseph P. Culver. 2011. “Imaging of Functional Connectivity in the Mouse Brain.” *PLoS ONE* 6(1):16322.

Williams, Alex H., Tony Hyun Kim, Forea Wang, Saurabh Vyas, Stephen I. Ryu, Krishna V. Shenoy, Mark Schnitzer, Tamara G. Kolda, and Surya Ganguli. 2018. “Unsupervised

Discovery of Demixed, Low-Dimensional Neural Dynamics across Multiple Timescales through Tensor Component Analysis." *Neuron* 98(6):1099-1115.e8.

Yu, Byron M., John P. Cunningham, Gopal Santhanam, Stephen I. Ryu, Krishna V. Shenoy, and Maneesh Sahani. 2009. "Gaussian-Process Factor Analysis for Low-Dimensional Single-Trial Analysis of Neural Population Activity." *Journal of Neurophysiology* 102(1):614–35.

Zhuang, Jun, Lydia Ng, Derric Williams, Matthew Valley, Yang Li, Marina Garrett, and Jack Waters. 2017. "An Extended Retinotopic Map of Mouse Cortex." *ELife* 6.